THE UNIVERSITY OF MANITOBA

DOSE DEPENDENT THEORY OF DAMAGE ACCUMULATION UNDER CASCADE IRRADIATION CONDITIONS

BY

NING LI

A THESIS SUBMITTED TO
THE FACULTY OF GRADUATE STUDIES OF
THE UNIVERSITY OF MANITOBA
IN PARTIAL FULFILLMENT OF THE REQUIREMENTS OF
THE DEGREE OF MASTER OF SCIENCE

DEPARTMENT OF PHYSICS
WINNIPEG, MANITOBA

January 1995

ISBN 0-612-13296-X

Canada

Name _____

Dissertation Abstracts International is arranged by broad, general subject categories. Please select the one subject which most nearly describes the content of your dissertation. Enter the corresponding four-digit code in the spaces provided.

Solid State

SUBJECT TERM

0	6	1	1

SUBJECT CODE

U·M·I

Subject Categories

THE HUMANITIES AND SOCIAL SCIENCES

COMMUNICATIONS AND THE ARTS

Architecture 0729
Art History 0377
Cinema 0900
Dance 0378
Fine Arts 0357
Information Science 0723
Journalism 0391
Library Science 0399
Mass Communications 0708
Music 0413
Speech Communication 0459
Theater 0465

EDUCATION

General 0515
Administration 0514
Adult and Continuing 0516
Agricultural 0517
Art 0273
Bilingual and Multicultural 0282
Business 0688
Community College 0275
Curriculum and Instruction 0727
Early Childhood 0518
Elementary 0524
Finance 0277
Guidance and Counseling 0519
Health 0680
Higher 0745
History of 0520
Home Economics 0278
Industrial 0521
Language and Literature 0279
Mathematics 0280
Music 0522
Philosophy of 0998
Physical 0523
Psychology 0525
Reading 0535
Religious 0527
Sciences 0714
Secondary 0533
Social Sciences 0534
Sociology of 0340
Special 0529
Teacher Training 0530
Technology 0710
Tests and Measurements 0288
Vocational 0747

LANGUAGE, LITERATURE AND LINGUISTICS

Language
- General 0679
- Ancient 0289
- Linguistics 0290
- Modern 0291

Literature
- General 0401
- Classical 0294
- Comparative 0295
- Medieval 0297
- Modern 0298
- African 0316
- American 0591
- Asian 0305
- Canadian (English) 0352
- Canadian (French) 0355
- English 0593
- Germanic 0311
- Latin American 0312
- Middle Eastern 0315
- Romance 0313
- Slavic and East European 0314

PHILOSOPHY, RELIGION AND THEOLOGY

Philosophy 0422
Religion
- General 0318
- Biblical Studies 0321
- Clergy 0319
- History of 0320
- Philosophy of 0322

Theology 0469

SOCIAL SCIENCES

American Studies 0323
Anthropology
- Archaeology 0324
- Cultural 0326
- Physical 0327

Business Administration
- General 0310
- Accounting 0272
- Banking 0770
- Management 0454
- Marketing 0338

Canadian Studies 0385
Economics
- General 0501
- Agricultural 0503
- Commerce-Business 0505
- Finance 0508
- History 0509
- Labor 0510
- Theory 0511

Folklore 0358
Geography 0366
Gerontology 0351
History
- General 0578
- Ancient 0579
- Medieval 0581
- Modern 0582
- Black 0328
- African 0331
- Asia, Australia and Oceania 0332
- Canadian 0334
- European 0335
- Latin American 0336
- Middle Eastern 0333
- United States 0337

History of Science 0585
Law 0398
Political Science
- General 0615
- International Law and Relations 0616
- Public Administration 0617

Recreation 0814
Social Work 0452
Sociology
- General 0626
- Criminology and Penology 0627
- Demography 0938
- Ethnic and Racial Studies 0631
- Individual and Family Studies 0628
- Industrial and Labor Relations 0629
- Public and Social Welfare 0630
- Social Structure and Development 0700
- Theory and Methods 0344

Transportation 0709
Urban and Regional Planning 0999
Women's Studies 0453

THE SCIENCES AND ENGINEERING

BIOLOGICAL SCIENCES

Agriculture
- General 0473
- Agronomy 0285
- Animal Culture and Nutrition 0475
- Animal Pathology 0476
- Food Science and Technology 0359
- Forestry and Wildlife 0478
- Plant Culture 0479
- Plant Pathology 0480
- Plant Physiology 0817
- Range Management 0777
- Wood Technology 0746

Biology
- General 0306
- Anatomy 0287
- Biostatistics 0308
- Botany 0309
- Cell 0379
- Ecology 0329
- Entomology 0353
- Genetics 0369
- Limnology 0793
- Microbiology 0410
- Molecular 0307
- Neuroscience 0317
- Oceanography 0416
- Physiology 0433
- Radiation 0821
- Veterinary Science 0778
- Zoology 0472

Biophysics
- General 0786
- Medical 0760

EARTH SCIENCES

Biogeochemistry 0425
Geochemistry 0996
Geodesy 0370
Geology 0372
Geophysics 0373
Hydrology 0388
Mineralogy 0411
Paleobotany 0345
Paleoecology 0426
Paleontology 0418
Paleozoology 0985
Palynology 0427
Physical Geography 0368
Physical Oceanography 0415

HEALTH AND ENVIRONMENTAL SCIENCES

Environmental Sciences 0768
Health Sciences
- General 0566
- Audiology 0300
- Chemotherapy 0992
- Dentistry 0567
- Education 0350
- Hospital Management 0769
- Human Development 0758
- Immunology 0982
- Medicine and Surgery 0564
- Mental Health 0347
- Nursing 0569
- Nutrition 0570
- Obstetrics and Gynecology 0380
- Occupational Health and Therapy 0354
- Ophthalmology 0381
- Pathology 0571
- Pharmacology 0419
- Pharmacy 0572
- Physical Therapy 0382
- Public Health 0573
- Radiology 0574
- Recreation 0575
- Speech Pathology 0460
- Toxicology 0383

Home Economics 0386

PHYSICAL SCIENCES

Pure Sciences

Chemistry
- General 0485
- Agricultural 0749
- Analytical 0486
- Biochemistry 0487
- Inorganic 0488
- Nuclear 0738
- Organic 0490
- Pharmaceutical 0491
- Physical 0494
- Polymer 0495
- Radiation 0754

Mathematics 0405
Physics
- General 0605
- Acoustics 0986
- Astronomy and Astrophysics 0606
- Atmospheric Science 0608
- Atomic 0748
- Electronics and Electricity 0607
- Elementary Particles and High Energy 0798
- Fluid and Plasma 0759
- Molecular 0609
- Nuclear 0610
- Optics 0752
- Radiation 0756
- Solid State 0611

Statistics 0463

Applied Sciences

Applied Mechanics 0346
Computer Science 0984
Engineering
- General 0537
- Aerospace 0538
- Agricultural 0539
- Automotive 0540
- Biomedical 0541
- Chemical 0542
- Civil 0543
- Electronics and Electrical 0544
- Heat and Thermodynamics 0348
- Hydraulic 0545
- Industrial 0546
- Marine 0547
- Materials Science 0794
- Mechanical 0548
- Metallurgy 0743
- Mining 0551
- Nuclear 0552
- Packaging 0549
- Petroleum 0765
- Sanitary and Municipal 0554
- System Science 0790

Geotechnology 0428
Operations Research 0796
Plastics Technology 0795
Textile Technology 0994

PSYCHOLOGY

General 0621
Behavioral 0384
Clinical 0622
Developmental 0620
Experimental 0623
Industrial 0624
Personality 0625
Physiological 0989
Psychobiology 0349
Psychometrics 0632
Social 0451

DOSE DEPENDENT THEORY OF DAMAGE ACCUMULATION UNDER CASCADE IRRADIATION CONDITIONS

BY

NING LI

A Thesis submitted to the Faculty of Graduate Studies of the University of Manitoba in partial fulfillment of the requirements of the degree of

MASTER OF SCIENCE

Acknowledgement

I am deeply grateful to my academic advisor Dr. C. H. Woo for his constant guidance and patience through all stages of this thesis work. His many creative ideas inspire my interest in the field of irradiation damage. Without his constructive suggestions this thesis would be impossible.

My special thanks are extended to Dr. J. M. Vail for his teaching and encouragement through all period of my study.

I would like to thank Dr. A. A. Semenov for his teaching of the theory of irradiation damage.

I am also thankful to the Reactor Materials Research Branch, Whiteshell Laboratories for hospitality during my stay.

I would like to acknowledge the financial support from COG.

Finally I would like to express my appreciation to my sister, Na Li, for her encouragement and support of my study.

Abstract

In reactor materials, the point defects are produced by energetic neutron irradiation. Not only does significant recombination of vacancies and interstitials occur, but also defects of like type form clusters under cascade irradiation conditions. The fact that primary vacancy clusters (PVCs) and primary interstitial clusters (PICs) have different thermal stabilities or lifetimes at elevated temperatures contributes to asymmetric defect accumulation in the medium. Consideration of this biased supply of free defect fluxes leads to the concept of production bias by Woo and Singh. On the basis of production bias theory, conservation equations of primary defect clusters in cascade regions are formulated. The dose dependence of the cluster concentrations and the void swelling has been calculated using numerical methods. It is found that the densities of PVCs and PICs and defect contents in the clusters initially increase rapidly with the dose, quickly reaching a quasi-steady state in which a dynamic equilibrium is maintained between creation by cascades and annihilation by different annealing processes. The maintenance of the equilibrium is attributed to the thermal evaporation of PVCs and the removal of PICs mainly by dislocation sweeping, glide of PICs and absorption of evaporated vacancies. The calculated results are consistent with previous studies and can be used to explain the observed high swelling behaviour at elevated temperatures.

CONTENTS

List of Figures

CHAPTER 1

INTRODUCTION

1.1 Origin of The Problem

The study of irradiation-induced void swelling in reactor materials began immediately following the discovery of this phenomenon in stainless steel in the middle of the sixties [1]. For the last three decades, the phenomenon of void swelling has been a subject of extensive theoretical and experimental investigation [2-11] because, apart from academic interest, it is also critical to the safe and economical operation of nuclear reactors. During the operation of a nuclear reactor, energetic particles, particularly fast neutrons are generated, which interact with and displace the atoms of the reactor components creating point defects--vacancies and interstitials, and their clusters. The diffusion and subsequent annihilation of these vacancies and interstitials at the existing microstructure of a metal or alloy cause new features such as voids and dislocation loops to appear and grow. These processes often

generate changes in the mechanical properties and the macroscopic dimensions of reactor materials, and in extreme cases, may seriously affect the efficient operation of a reactor, unless the processes are controlled or affected alloy parts replaced.

Microstructural evolution in irradiated materials has traditionally been analyzed using a chemical reaction rate theory in which the generation rate of the point defects is estimated by the NRT displacement model (Norgett-Robinson-Torrens) [12]. It is implicitly assumed that during irradiation: (a) interstitials and vacancies are produced in the form of Frenkel pairs continuously in time and uniformly in space, and these defects are available for the interaction with existing sinks in the medium such as dislocations, voids and grain boundaries. (b) the preferential attraction of self-interstitial atoms (SIAs) to existing dislocations (dislocation bias) is the only factor in creating a segregation between the vacancies and SIAs, and hence the accumulation of the irradiation damage.

This conventional rate theory can be successfully applied in the cases where the irradiation damage is created in the form of single-displacements (e.g. in 1 Mev electron and low energy light ion irradiations). However, as noted by several authors, it does not provide sufficient information to fully understand the irradiation damage process when displacement cascades are present (e.g. in fission and fusion neutron and high energy heavy ion irradiations). In such cases, the interactions of projectile particles with the

atoms in the material are much more complicated and the irradiation damage takes place in the form of multi-displacements [fig. 1.1].

1.2 Nature of Cascade Damage

It is important to understand the process of cascade collision to correctly represent the physics of material property change due to cascade irradiation. Let us use a simplified model [13] to qualitatively describe what happens during a cascade collision. The model is based on the following assumptions.

* Atoms in collision behave like hard spheres.

* All collisions are elastic and no energy is dissipated in electron excitation.

* The cascade proceeds as a series of two-body collisions.

* Those collisions are independent of each other and any spatial correlations implied by the periodicity of the crystal structure can be ignored.

* In a collision, after a recoil atom with energy E interacts with the lattice, the atom emerges with E_1 and generates a new recoil with E_2. It is assumed that no energy passes to the lattice and

$$E = E_1 + E_2$$

* A stationary atom which receives less than a critical energy E_d is not displaced. Similarly if an incident atom emerges from collision with $E_1 < E_d$, it does not contribute further to the cascade. These statements form the definition of the *threshold displacement energy* E_d. For simplicity we shall

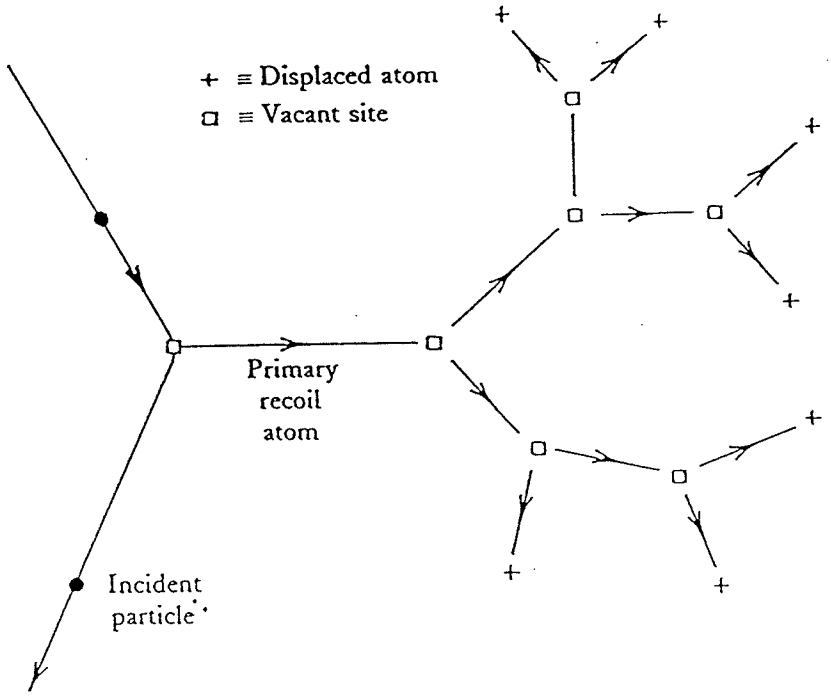

Fig.1.1 The multiple displacement in the core of cascade region (after M.W. Thompson [13]).

take the probability of displacement to be zero below E_d, rising sharply to 1when E is equal to or greater than E_d.

1.2.1 Primary Knock-on Event And Single-displacement

Interaction between irradiation and solid can be conveniently divided into two steps: the first is the interaction of the incident particle of energy E with the stationary nucleus of a lattice atom. If the particle possesses sufficient energy (normally it does), the atom can be displaced from its original site by acquiring a certain recoil energy from the incident particle. The atom is described as the *primary knock-on atom* (PKA). In the second step, the mobile PKA recoils and is capable of displacing additional lattice atoms known as secondary and higher generation knock-on atoms. Eventually the PKA stops when its recoil energy is less than the threshold displacement energy E_d. The entire process is defined as the primary knock-on event. The most important feature of the primary knock-on event is the energy transfer to the PKA. The PKA has an energy spectrum varying from zero to a certain maximum value depending on the energy and nature of the incident particle and of the lattice atom. In the elastic collision approximation, for instance, according to the laws of conservation of energy and momentum, the energy transfer to the PKA is defined as

$$E = \frac{4M_1M_2E_0}{(M_1+M_2)^2}\sin^2(\theta/2) \qquad (1.1)$$

where E_0 is the energy of the incident particle, M_1 and M_2 are the masses of the incident particle and of the lattice atom, respectively, and θ is the angle between the paths of incident particle and of recoil atom. The maximum possible energy is transferred at the moment of a head-on collision ($\theta = 180^0$). The interaction of irradiation with atoms is generally considered from the viewpoint of the scattering particle. The cross-sections of interaction are known from nuclear physics and can be taken from available sources.

If the PKA's recoil energy E is small (e.g. < 30 eV), only single-displacement takes place. It yields a single interstitial-vacancy pair, or Frenkel pair. A good impression about the dynamics of such a displacement event is obtained from dynamic computer simulation studies where the motion of the atoms in a small crystal is calculated after one of the atoms has received an energetic recoil [14,15]. In a single-displacement event, the damage accumulation in reactor materials has been successfully described on the basis of the NRT model.

1.2.2 Displacement Cascade

In most of the cases relevant for reactor materials, i.e. under fast fission and fusion irradiation with MeV neutrons, high recoil energies in the keV range

are transferred to PKAs, and the energetic PKAs can therefore further displace additional atoms during their slowing down in the lattice, resulting in the generation of secondary knock-on atoms and so on. The result is a displacement cascade whose formation mechanism has been studied by computer simulation using the binary collision approximation [16-18] and in more detail by molecular dynamics calculations [19-22].

The sequence of cascade events can be characterized as follows: the first step is a local explosion within a few tenths of a picosecond where the kinetic energy of the PKA is rapidly distributed over a large number of lattice atoms in close proximity. A number of atoms is transported directly or via displacement sequences from the centre of the primary knock-on event to the periphery, forming interstitial atoms. Their previous sites become vacant. After a number of displacements, the energy of the colliding atoms would have dissipated so much that they are no longer able to transfer enough energy to displace their neighbours. Thus, these displacement events cease, resulting in a vacancy-rich core surrounded by a halo of interstitials (fig. 1.2). Atoms which are still in this disordered cascade region are in a highly agitated state, and this region can be visualized as a highly superheated and compressed melt. Atoms in the centre of the cascade region have energies far in excess of 1 eV (i.e. an equivalent temperature of 10^4 K). The excess kinetic energy in this superheated melt is then dissipated quickly into the surrounding matrix through heat conduction and the creation and propagation of phonons, in a period

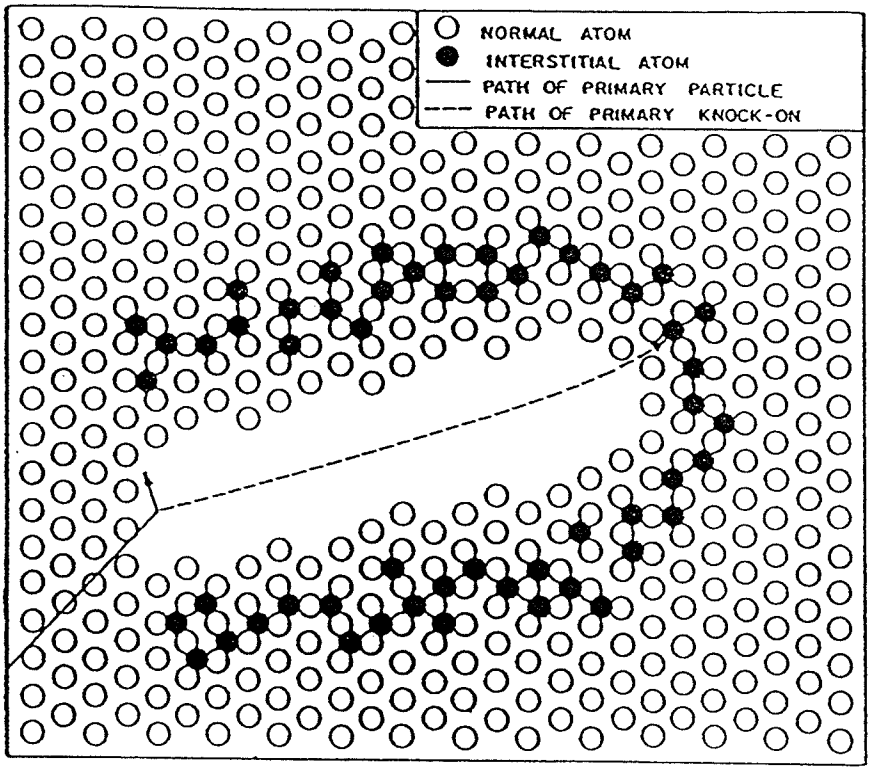

Fig.1.2 The collision cascade shown schematically (after M.W. Thompson[13]).

from a few tenths of a picosecond to several picoseconds which is called the the cooling-down phase. As this superfast quenching takes place, the melt recrystallizes from the periphery to the centre. A net number of vacant latticesites corresponding to the net number of atoms ejected into the surrounding crystalline matrix then condense into one or more vacancy clusters in the centre of the cascade. Concurrently the ejected atoms agglomerate and form interstitial clusters in the peripheral region of cascades. At the same time, extensive atomic rearrangement leads to defect annihilation by recombination of vacancies and interstitials. After several picoseconds the cascade has returned to ambient temperature. Of particular interest to us are the interstitial clusters formed at the periphery of the cascades.

For very energetic PKAs, with the primary recoil energy above about 15 to 20 KeV, the cascades tend to split up into subcascades which themselves contain a very high local vacancy and interstitial densities. The reason for the appearance of subcascades is the increased distance travelled by a very energetic PKA between the generation of two energetic secondary recoil atoms. If this distance is larger than the dimensions of the subcascades produced by the secondary recoil atoms, the subcascades can then be regarded as separate units. The splitting up into subcascades can be observed experimentally in self-ion irradiated gold [23] with a gold projectile of energy E_0. Under the transmission electron microscope one would recognize that, up to 100 keV Au ion irradiation, more than half of the cascades in Au are split up into two or

more and up to 200 keV into four or more subcascades. The characteristics of the subcascades presumably resemble those of individual cascades described above.

If the ambient temperature is sufficiently high for thermal mobility, point defects and sometimes small defect clusters will be released from cascade regions into the surrounding matrix. Defect clusters formed in cascades will subsequently grow or shrink by absorption of point defects of like or opposite type and by thermal emmision of point defects. Because of the randomness of these events, the sizes of individual clusters will undergo significant fluctuations over time.

An important factor characterizing the structure of radiation damage is the cascade volume which may be defined as the volume containing all the colliding atoms. An analytical theory of the energy deposition in an amorphous solid [24] predicts the average volume in which the recoil energy is dissipated to be roughly proportional to E^2. Experimentally the size of displacement cascades produced by energetic copper ions in an ordered Cu_3Au alloy could indirectly be observed. The technique uses the superlattice reflection to image the local regions of disorder in an electron microscope. The experimentally measured d, which is the average linear dimensions of these disordered regions, as a function of the recoil energy E is in good agreement with the theoretical predictions. As a typical value one finds that a PKA of 50 keV produces a cascade of about 7 nm diameter [25].

Recent studies [26,27] have shown that, under cascade damage conditions, vacancies and interstitials are produced in a localized and segregated fashion, and can be immobilized in the form of primary vacancy clusters (PVCs) and primary interstitial clusters (PICs). These are due to the high defect concentrations in the cascade region during the cooling down phase of the cascade core. The effects of the production of PVCs in the cascade region was first considered in a rate theory treatment of void swelling by Bullough, Eyre and Krishan [28]. Subsequently, Heald and Speight [29] and Foreman and Makin [30] also calculated the effect of PVCs in void swelling, and found that consideration of PVCs in the cascade region did not cause much change in the magnitude of swelling. The dislocation bias was still considered to be the sole driving force for void swelling and growth. Only recently, the evidence of clustering of interstitials has been accumulating. Experimental results obtained by diffuse X-ray scattering have suggested the spontaneous formation of interstitial clusters in the cascade volume [31,32]. Using a diffusion-based methodology, Woo, Singh and Heinish have shown that a significant fraction of interstitials produced in a cascade may be immobilized in the form of clusters [33]. Molecular dynamics (MD) investigations also give evidence of clustering of interstitials produced in the cascade region during the cooling-down phase of the cascade [19,34].

1.3 Production Bias

Recently, Woo and Singh [26] considered the effects of both PVCs and PICs in the rate theory treatment of irradiation damage under cascade damage conditions. They have shown that at elevated temperatures vacancies would evaporate from vacancy clusters and most of them would escape into the medium. The interstitial clusters, on the other hand, are thermally more stable due to their higher binding energy and thus remain immobilized in the form of clusters until they are removed by interacting with growing loops and climbing dislocation segments or annihilated by the excess vacancies. This asymmetric effective point defect supply at high temperatures between vacancies and interstitials results in a large increase in the vacancy accumulation in voids. From the consideration of segregated production of PVCs and PICs and the difference of their thermal stabilities or lifetimes, the concept of *production bias* has been proposed and developed by Woo and Singh to supplement the conventional rate theory. In the conventional rate theory, the homogeneous generation of vacancies, and interstitials during irradiation and the assumption of the dislocation bias as the only driving force for void swelling is inconsistant with many experimental explanations, particularly when the large intracascade recombination is taken into account [35]. This concept was first tested in the study of void swelling by Woo and Singh [26,27], Singh, Woo and Foreman [36], and dislocation climb and interstitial loop growth by Woo and Semenov [37] in the steady state. The results are in good accord with the available experimental measurements [38]. More recent applications to irradiation creep

and growth [35,39-42] also result in the successful explanation of a number of complicated phenomena which have been inexplicable thus far.

In addition, it is worthwhile to note that the defect clusters do not only act as sources of point defects, but also as sinks of point defects. Effectively, they reduce the average number of defect jumps between creation and annihilation which, in turn, reduce their contribution to the damage accumulation in the matrix. At low temperature, defect clusters are predominantly sinks and at high temperature they can be predominantly sources by emitting point defects, particularly the PVCs. The difference between PVCs and PICs in the capacity as point-defect sources depends on the temperature [43].

1.4 Aim of The Study

1) The study of damage accumulation facilitates the test of the new concept of *production bias* resulting from an asymmetrical generation of primary defect clusters and their different lifetimes at elevated temperatures. Production bias has recently been incorporated by Woo et al [26-27,35-44] into the traditional rate theory to investigate the microstructural evolution under cascade damage conditions. In order to give a sound explanation to the experimentally observed high void swelling rate at elevated temperature range, the mechanism of creation and annihilation of both PVCs and PICs, which contribute mostly to the void swelling, has to be investigated. On the other

hand, correct prediction of theoretical model helps in the design and analysis of reactors and experiments.

2) The study of damage accumulation assists the verification of the solution to the problem of cluster evolution and void swelling under cascade conditions. The problem can theoretically be tackled using the Fokker-Planck method [43,44], and if the loop number density is known, it can also be considered using the chemical reaction kinetic theory. It is desirable to supplement the Fokker-Planck method by a simpler rate theory based method of analysis.

3) The study of damage accumulation helps the fundamental understanding of the nature of cascade damage and the cascade collapse to form defect clusters [45]. Cascades can not be directly observed experimentally owing to the spatial and temporal limits of resolution of experimental techniques such as electron microscopy and field-ion microscopy. Typically, cascades have dimensions of nanometres and lifetimes of picoseconds. Therefore indirect observation is usually based on imaging defect accumulations that arise from the cascades; for example, void swelling. The modelling of the void swelling from the collapse of displacement cascades and the comparison of calculated results with experimental observation is one of the effective methods of checking theoretical cascade models [46].

4) The study of damage accumulation increases our understanding of microstructural evolution and macroscopic property change (dimensional,

physical, electrical and mechanical) of reactor materials due to irradiation. In engineering applications, the microstructural data and the understanding provide the knowledge needed to select or develop more radiation-resistant, high-performance materials in fast fission reactors and future fusion reactors.

5) The accumulation of point defect clusters is one of the main causes of irradiation-induced embrittlement due to hardening. The study of the time evolution of the point-defect clusters is useful in understanding this important cause of irradiation-induced degradation of nuclear materials.

CHAPTER 2

DYNAMICS OF PRIMARY DEFECT CLUSTERS

2.1 Effective Point Defect Generation Rate

During the past decade, transmission electron microscope (TEM) investigations of irradiated materials have demonstrated that the accumulation of defects (i.e. interstitials and vacancies) under cascade damage conditions does not occur homogeneously in space, as it is commonly perceived. The common perception has its origin in the assumption that even under cascade damage conditions, the defects are produced uniformly in space and time and in the form of single Frenkel pairs. With this assumptions and the use of mean-field approach, chemical reaction rate equations are used to calculate the rate of defect accumulation. Within this framework, the problem of localization and segregation of defects cannot be understood. The evidence, therefore, that the accumulation of both interstitials and vacancies occurs in a

segregated fashion, would strongly suggest that the conventional rate theory approach may not be adequate for treating the problem of defect accumulation under cascade damage conditions. During cascade damage, the energetic primary knock-on atom distributes the damage energy (PKA energy minus the cumulative inelastic losses) through a quick succession of generation of secondary knock-on atoms and replacement collisions in a few tenths of a picosecond within a small region of the crystal. The highly disordered state, and the density of kinetic energy (exceeding significantly that of molten material at the melting temperature) in the central region of the cascade, suggests that this region at the end of the collisional phase, is best described as a highly superheated melt under compression. The fact that displacement collisions eject atoms in the central core of cascade into the surrounding crystal results in a vacancy-rich core in the cascade surrounded by a halo of net interstitials. Portions of the ejected atoms with enough kinetic energies also escapes from the cascade region and enters into the matrix as freely migrating defects. During the cooling-down phase, defect configurations rearrange. This includes recombination between opposite types of defects as well as clustering of like defects. Vacancy clusters form predominately in the central region, whereas interstitial clusters form mainly in the periphery of the cascade. According to this mechanism of defect production, Woo and Singh have proposed that to model cascade damage effects, initial cascade damage displacement must include at least three portions: (a) those which annihilate by

the recombination of opposite types, (b) those which cluster with like type and then evaporate from clusters at elevated temperatures and (c) those which escape the cascade region as freely migrating defects (including small mobile clusters) and annihilate in the sinks or recombine with the opposite type defects after long range migration. It is very clear that this enhanced rate theory not only considers defect recombination and diffusion in the medium as conventional theory does, but also sorts out a portion which engages in the formation of defect clusters among all point defects produced in cascade irradiation, and also considers the effects of the continuously produced clusters which act as both sinks and sources of the mobile point defects.

Therefore, the total atomic displacement rate K (dpa/s), calculated with the NRT model [12], can be divided into three portions according their final status under cascade irradiation conditions:

$$K= \alpha K+ \lambda_i K+ \mu_i K \tag{2.1}$$

$$K= \alpha K+ \lambda_v K+ \mu_v K \tag{2.2}$$

Each atomic displacement can be thought of producing a nascent Frenkel pair. In the first terms of equations (2.1) and (2.2), α is the fraction of displacements which anneal through recombination. As mentioned in the chapter of the introduction the concentration of nascent point defects in the cascade region is high, and there is a high possibility for an interstitial to fall

into a vacancy and become a normal atom in the crystal lattice. Obviously, the annealed portion of the displacement damage does not contribute to irradiation damage effects such as void swelling or creep. Previous work [27] has shown that the amount of recombination accounts for a substantial portion (~90%) of the initial displacements owing to high nascent point-defect concentration in the cascade volume.

In the second terms, $\lambda_j(j=i,v)$ is the fraction of point defects which cluster. The clusters formed provide new sinks in addition to the conventional ones - dislocations, voids, grain boundaries and surfaces. Clusters grow by acquisition of freely migrating defects of the same type, and shrink by the absorption of the opposite type of defects. $\lambda_j(j=i,v)$ that denotes the amount of clustering has a special importance in the evolution of microstructure under cascade conditions. It is also a key factor in cascade processes, which the traditional rate theory model does not describe accurately.

$\mu_j(j=i,v)$ is the fraction of point defects which escape the cascade region and annihilate at various sinks or recombine with defects of the opposite type after long range migration. This portion of point defects actually includes small mobile defect clusters such as di-, tri- and tetra-point defect clusters since these small clusters are of comparable migrating energy with single point defects. Since vacancies and interstitials are produced in equal numbers and the subsequent mutual recombination of produced point defects in the cooling-down phase of cascade core annihilates the same amount of vacancies and

interstitials, $(\lambda_i K+\mu_i K)$ is the same as $(\lambda_v K+\mu_v K)$ from equations (2.1) and (2.2). However, the interstitial clustering fraction $\lambda_i K$ is not likely to be the same as the vacancy clustering fraction $\lambda_v K$ because of the different formation and binding energies of interstitials and vacancies. Also, there might be more or fewer interstitials in an interstitial cluster than vacancies in a vacancy cluster, or there might be more or fewer interstitial clusters formed than vacancy clusters formed. As will be explained later, some vacancies will evaporate from vacancy clusters at elevated temperatures and escape from the cascade area. These vacancies participate in the irradiation damage process through interactions with the sinks. On the other hand, interstitials are stable in their clusters owing to the high thermal stability until a much higher temperature. It is important to note that it has not been previously realized that it is not the displacement rate K, but rather $\mu_v K$ and some of $\lambda_v K$ which contribute to the accumulation of vacancies in voids and make significant void swelling possible at the peak swelling temperature range.

Because the mutual recombination at cascade core accounts for a very large proportion of the initial displacements, it is necessary to define an effective point-defect production rate which bears a correct relationship with the microstructural evolution of the material. Woo and Singh [26] defined an *effective point defect generation rate* G by

$$G = (1 - \alpha)\, K \tag{2.3}$$

It is clear that G is the generation rate of all the point defects that are available to contribute to the rate of defect accumulation in the matrix during cascade damage conditions. Let

$$\varepsilon_j = \lambda_j/(1-\alpha); \quad j=i,v \tag{2.4}$$

then the rate at which point defects are immobilized in clusters is given by

$$\lambda_j K = \varepsilon_j G; \qquad j=i,v \tag{2.5}$$

and the production rate of the mobile defects capable of undergoing long-range migration is thus

$$\mu_j K = (1-\varepsilon_j)G; \quad j=i,v \tag{2.6}$$

It should be emphasized that at the peak swelling temperature, the supersaturation of vacancies which is the main driving force for void swelling arises from two sources: (a) vacancies evaporating from the vacancy cluster at the cascade core and (b) freely migrating vacancies. Furthermore, an analysis of the existing evidence clearly suggests that the former causes a far greater imbalance (bias) of the flux of free vacancies to sinks, than the latter.

2.2 Derivation of The Equations Governing Primary Defect Clusters and Void Swelling

In this thesis, the kinetics of irradiation induced point defects is analysed using chemical reaction rate equations. The equations for the steady state interstitial and vacancy concentrations C_i and C_v, respectively, can be written by using equations (2.1) and (2.2);

$$(1-\varepsilon_i)G-[k_c^2+(1+p)k_d^2]D_iC_i-\alpha_tC_iC_v=0 \qquad (2.7)$$

$$(1-\varepsilon_v)G-[(k_c^2+k_d^2)D_vC_v - K^e]-\alpha_tC_iC_v=0 \qquad (2.8)$$

The first terms in equations (2.7) and (2.8) represent the effective production rates of freely migrating point defects in the medium. The second terms represent the annihilation rates of produced point defects at different sinks (such as voids, network dislocations, interstitial loops and vacancy or interstitial clusters). The third terms represent the rate of annihilation due to mutual recombination of freely migrating vacancies and interstitials which escape the cascade volume.

In the present case under fast reactor conditions ($K\sim10^{-6}$ dpa/s and $300°C<T<700°C$) [42] for the 316 stainless steel, it is a good assumption to neglect the effect of recombination αC_iC_v. The steady state void swelling rate dS/dt has successfully been derived from equations (2.7) and (2.8) by Woo,

Singh and Semenov [26,37] under two opposite considerations: (a) from the rate of vacancy accumulation in voids; (b) from the net interstitial flux to the interstitial loops and network dislocations. These two approaches produce the same result as below, which clearly demonstrates the consistency of the present approach.

$$\frac{dS}{dt} = \frac{k_c^2}{k^2}(\epsilon_i - \epsilon_v')\,G + p(1-\epsilon_i)\,\frac{k_c^2 k_d^2 G}{k^2(k^2 + pk_d^2)} - K_c \qquad (2.9a)$$

with $$S_{t=0} = (4\pi r_{c0}^3/3)N_c \qquad (2.9b)$$

where G is the effective point defect generation rate in equation (2.3), p is the dislocation bias which represents the effect of preferential absorption of free interstitials (compared to vacancies) by dislocations, ε_i is the intracascade interstitial clustering fraction, ε_v is the intracascade vacancy clustering fraction, ε_v' is related with ε_v and will be defined later. k^2 is called the sink strength and is a measure of the total ability of a sink-type to absorb point defects. Here k_c^2 is the sink strength of the voids. The subscript c refers to cavities in general including voids. The symbol for voids is used to avoid confusion with vacancies. k^2 is the total sink strength for vacancies, K_c is the vacancy emission rate from voids, N_c is the number of voids per unit volume.

In equation (2.9b) r_{c0} is the initial average radius of voids. In the calculation, r_{c0} is reasonably set at 15×10^{-10} meter. Actually, our computed results

are not significantly affected within the range of r_{c0}=(10 to 30)×10^{-10} metres.

To include the effect of production of PICs and PVCs on steady-state swelling, the conservation equations for the primary defect clusters had been derived by Woo and Semenov [37]. Accordingly, the atomic concentrations N_{ic}, N_{vc} of PICs, PVCs and total defect contents Q_i, Q_v in the PICs and PVCs at any time t are given in the form of first order nonlinear differential equations,

$$\frac{dN_{ic}}{dt} = \frac{\epsilon_i G}{n_{i0}} - \theta(\tau_i^s)\frac{N_{ic}}{\tau_i^s} - \frac{N_{ic}}{\tau_i^d} \qquad (2.10a)$$

$$\frac{dQ_i}{dt} = \epsilon_i G - \frac{2r_{i0}N_{ic}n_i}{r_i\tau_i^s} - \frac{N_{ic}n_i}{\tau_i^d} \qquad (2.11a)$$

$$\frac{dN_{vc}}{dt} = \frac{\epsilon_v G}{n_{v0}} - \theta(\tau_v^s)\frac{N_{vc}}{\tau_v^s} - \frac{N_{vc}}{\tau_v^d} \qquad (2.12a)$$

$$\frac{dQ_v}{dt} = \epsilon_v G - \frac{2r_{v0}N_{vc}n_v}{r_v\tau_v^s} - \frac{N_{vc}n_v}{\tau_v^d} \qquad (2.13a)$$

with initial conditions:

$$N_{ic}(t=0)=0 \qquad (2.10b)$$

$$Q_i(t=0)=0 \qquad (2.11b)$$

$$N_{vc}(t=0)=0 \qquad (2.12b)$$

$$Q_v(t=0)=0 \qquad (2.13b)$$

where the first terms on the right-hand side of equations (2.10a) and (2.12a) are the generation rates of PICs and PVCs directly by cascades. In reality, there is a distribution of cluster sizes, but for simplicity it is assumed here that they are all of the same average size. The second terms are the loss rates of PICs and PVCs due to shrinkage caused by an unbalanced absorption of freely migrating vacancies or interstitials. The third terms represent the loss rates of PICs and PVCs due to absorption by dislocations. In equations (2.11a) and (2.13a) the first terms are the generation rates of interstitial contents and vacancy contents in their respective clusters directly by cascades. The second and third terms have similar meaning to the corresponding terms in equations (2.10a) and (2.12a). n_{j0} (j=i,v) is the defect content of a PIC or PVC on creation, n_j (j=i,v) is the mean point defect contents of a PIC or PVC. τ_j^s (j=i,v) is the lifetime of a PIC or PVC between its creation and annihilation due to shrinkage caused by an unbalanced absorption of freely migrating vacancies or interstitials. Throughout this thesis all concentrations or densities are atomic fractions and the production rates are numbers of defects per atom per second. To ensure that the lifetimes τ_i^s and τ_v^s in the equations (2.10a) and (2.12a) are positive and physically meaningful , Woo and Semenov [37] have also used the step function,

$$\theta(\tau_j^s)= \begin{cases} 0 & (\tau_j^s \le 0) \\ 1 & (\tau_j^s > 0) \end{cases} . \qquad (2.14)$$

The mean point defect content n_j (j=i,v) and void swelling S in the equation (2.9a)

can be further expressed as,

$$n_j=\pi b r_j^2/\Omega \quad (j=i,v) \tag{2.15}$$

$$S=(4\pi r_c^3/3)N_c \tag{2.16}$$

in which b is the Burger's vector for dislocation loops, r_j (j=i,v) is the mean radius of the PICs or PVCs, Ω is the atomic volume, r_c is the average radius of voids. In the equations (2.10a) to (2.13a), τ_j^d (j=i,v) is the combined lifetime of the primary clusters between their creation and absorption at dislocations. Lifetimes τ_j^s and τ_j^d are related with the flux of free interstitials and vacancies as following,

$$(\tau_i^s)^{-1}=-\frac{\Omega}{br_{v0}}(J_{i0}-J_{v0}+J_{ic}^e) \tag{2.17}$$

$$(\tau_v^s)^{-1}=\frac{\Omega}{br_{v0}}(J_{i0}-J_{v0}+J_{vc}^e) \tag{2.18}$$

$$(\tau_j^d)^{-1}=(\rho_N+\rho_{il})W_j; \quad (j=i,v) \tag{2.19}$$

where W_j is the reaction constant between dislocation line segments and PICs or PVCs in which the difference between W_i and W_v can be neglected [43], ρ_N and ρ_{il} are the total network dislocation density and total interstitial loop line density, respectively. J_{j0} (j=i,v) is the steady-state flux of free interstitials or vacancies

which arrive on a dislocation line segment of unit length, and J_{jc}^{e} (j=i,v) is the vacancy emission strength of the PICs or PVCs. J_{j0} and J_{jc}^{e} can be expressed as,

$$J_{i0}=ZG(1+\bar{p})(1-\varepsilon_i)/(k^2\Omega) \tag{2.20}$$

$$J_{v0}=ZG(1-\varepsilon_v')/(k^2\Omega) \tag{2.21}$$

$$J_{ic}^{e}=ZD_vC_{ic}^{e}/\Omega \tag{2.22}$$

$$J_{vc}^{e}=ZD_vC_{vc}^{e}/\Omega \tag{2.23}$$

in which the vacancy diffusion coefficient is given by $D_v=D_{v0}\exp[-E_v^m/kT]$ [48]. D_{v0} is the vacancy diffusivity pre-exponential, E_v^m is the vacancy migration energy. In equations (2.20) to (2.23) Z is the dislocation bias factor for vacancies. C_{jc}^{e} is the equilibrium concentration of vacancies in the neighbourhood of an interstitial or vacancy cluster. $\bar{p}$ will be defined later. k^2 is the total sink strength for the capture of vacancies which is equal to the sum of sink strengths of voids and all dislocations,

$$k^2=k_c^2+k_d^2 \tag{2.24}$$

where k_d^2 includes the contribution from various dislocation types,

$$k_d^2=k_N^2+k_{il}^2+k_{ic}^2+k_{vc}^2\ . \tag{2.25}$$

In equations (2.24) and (2.25), k_c^2, k_N^2, k_{il}^2, k_{ic}^2 and k_{vc}^2 are the sink strengths for vacancies of the voids, network dislocations, interstitial loops, interstitial clusters and vacancy clusters respectively; N_c, N_{il}, N_{ic}, N_{vc} are corresponding densities and r_c, r_{il}, r_{ic}, r_{vc} are corresponding average radii. The various sink strengths can also be expressed in terms of the densities and sizes of the respective sinks in the material as follows,

$$k_c^2=4\pi r_c N_c/\Omega \tag{2.26}$$

$$k_N^2=Z\rho_N \tag{2.27}$$

$$k_{il}^2=2\pi r_{il} N_{il} Z/\Omega \tag{2.28}$$

$$k_{ic}^2=2\pi r_{ic} N_{ic} Z/\Omega \tag{2.29}$$

$$k_{vc}^2=2\pi r_{vc} N_{vc} Z/\Omega \ . \tag{2.30}$$

The derivation of the expressions for the above sink strengths can be found in Brailsford and Bullough's work [49]. In equations (2.20) and (2.21), Woo and Semenov have defined,

$$\bar{p}=pk_c^2/(k^2+pk_d^2) \tag{2.31}$$

$$\varepsilon_v'=\varepsilon_v - K^e/G \tag{2.32}$$

in which K^e is the rate of thermal vacancy emission from all the sinks which can

emit vacancies. Therefore ε_v' includes the effect of thermal instability of vacancies in various sinks,

$$K^e=K_c+K_N+K_{il}+K_{ic}+K_{vc} \ . \tag{2.33}$$

In equation (2.33), K_c, K_N, K_{il}, K_{ic}, K_{vc} are the vacancy emission strengths, contributed from voids, network dislocations, interstitial loops, interstitial clusters and vacancy clusters respectively. Normally, vacancy emission strength K can be related with sink strength k^2 in terms of vacancy diffusion coefficients and the thermaldynamic equilibrium vacancy concentrations in the immediate neighbourhood of the sink [45],

$$K_c=k_c^2D_vC_c^e \tag{2.34}$$

$$K_N=k_N^2D_vC_N^e \tag{2.35}$$

$$K_{il}=k_{il}^2D_vC_{il}^e \tag{2.36}$$

$$K_{ic}=k_{ic}^2D_vC_{ic}^e \tag{2.37}$$

$$K_{vc}=k_{vc}^2D_vC_{vc}^e \tag{2.38}$$

where C_c^e, C_N^e, C_{il}^e, C_{ic}^e, C_{vc}^e are the equilibrium concentrations of vacancies in the neighbourhood of voids, network dislocations, interstitial loops, interstitial clusters and vacancy clusters respectively, and these concentrations are related with the various activation energies as below,

$$C_c^e = C_0^e \exp[(2\gamma/r_c - P_g)\Omega/kT] \quad (2.39)$$

$$C_N^e = C_0^e = \exp[-E_v^f/(kT)] \quad (2.40)$$

$$C_{il}^e = C_0^e = \exp[-E_v^f/(kT)] \quad (2.41)$$

$$C_{ic}^e = C_0^e \exp[-\Delta E/(kT)] \quad (2.42)$$

$$C_{vc}^e = C_0^e \exp[\Delta E/(kT)] \quad (2.43)$$

where γ is the surface free energy, E_v^f is the vacancy formation energy, ΔE is the average loop-line energy, k is Boltzman's constant and T is the absolute temperature. Since network dislocations and interstitial loops both have the dislocation character of their perimeters, it is assumed that they have the same preference for interstitials. The effect of gas pressure P_g in voids is neglected in the calculation due to the unknown concentration of gas atoms and the complex interaction between vacancies and various gas atoms in voids. From this approximation, we expect a lower concentration of voids and smaller void swelling in our calculation than it should be because gas atoms serve as nucleating agents for cavities and resist the shrinkage of voids, in particular, at high temperatures and fusion environment where the production rate of gas atoms such as helium in the medium increases dramatically.

The steady-state problem has been solved previouly and found to describe the temperature dependence of both steady-state void swelling [37] and irradiation growth [39] very well. The time-dependent problem has not been solved as mentioned in the introduction. This is the purpose of the present thesis.

CHAPTER 3

NUMERICAL SCHEME

3.1 Introduction

The vast majority of mathematical formulations describing physical processes cannot be solved analytically. The only way to obtain a description of the behaviour of a solution is to approximate the problem in such a way that numerical representation of the solution can be produced. The process of obtaining a numerical solution is then reduced to a series of arithmetic operations and such a process is called a **numerical method** [50].

The most important mathematical model for physical phenomena is the differential equation. Motion of objects, fluid, and heat flow, bending and cracking of materials, vibrations, chemical reactions, and nuclear reactions are all modeled by differential equations. A differential equation is an equation involving one or more dependent variables, their derivatives (possibly of higher order) and

one or more independent variables. A differential equation with one independent variable is called an **ordinary differential equation** (ODE). A differential equation with more than one independent variable is called a **partial differential equation** (PDE). The order of a differential equation is the highest order of any of the derivatives in the equation.

The present problem, involving the evolution of defect clusters and void swelling, is represented by a system of ordinary differential equations (ODEs). Since it has to be solved by numerical means, a brief description of the principle of solving ODEs with numerical method will be introduced next. In fact, as the computer technology develops rapidly, numerical methods or numerical analysis are becoming increasingly important in scientific and engineering applications. Much literature about numerical methods is available for detail reference.

3.2 Numerical Methods for ODEs.

The five equations (2.9) to (2.13) in chapter two are typical coupled first order ordinary differential equations with the general form [51],

$$dy_i(x)/dx = f_i(x, y_1, ..., y_n), \qquad i= 1, ..., n \qquad (3.1)$$

and initial conditions

$$y_i(a)=y_{i,0}, \qquad i=1,...,n, \quad a<x. \qquad (3.2)$$

where the functions f_i on the right-hand side are given, x is the independent variable and the $y_{i,0}$ are given initial conditions.

A problem involving ordinary differential equations (ODEs) is not completely specified by its equations. Even more crucial in determining how to attack the problem numerically is the nature of the problem's boundary conditions. In general they can be satisfied at discrete specified points, but do not hold between those points, i.e. are not preserved automatically by the differential equations. Boundary conditions can be as simple as requiring that certain variables have certain numerical values, or as complicated as a set of nonlinear algebraic equations among the variables.

Usually, it is the nature of the boundary conditions that determine which numerical methods will be feasible. Boundary conditions are divided into two broad categories.

* In initial value problems, all the y_i are given at some starting value x_s, and it is desired to find the y_i at some final point x_f, or at some discrete list of points.

* In two-point boundary value problems, on the other hand, boundary conditions are specified at more than one x. Typically, some of the conditions will be specified at x_s and the reminder at x_f.

In the present study an initial value problem of five equations with right-hand side functions f given at beginning time x=0 has been derived.

The underlying principle of any routine for solving the initial value

problem involves approximating the infinitesimal dy's and dx's in (3.1) by finite differences Δy and Δx, and multiplying the equations by Δx. This gives algebraic formulas for the change in the functions when the independent variable x is "stepped" by one "stepsize" Δx. In the limit of making the stepsize very small, a good approximation to the underlying differential equation is achieved. Theoretically, as the stepsize continues to reduce, the solution approaches the exact solution with arbitrary accuracy. According to the above principle, a flow chart could be set up (fig.3.1) and a computer program could be written accordingly to attack the system of equations (3.1) and (3.2).

The choice of a suitable numerical method is now considered. There are several numerical methods available for solving initial value problems for ODEs, the most popular ones being:

* Runge-Kutta method.
* Richardson extrapolation (and its particular implementation as the Bulirsch-Stoer method).
* predictor-corrector method.

It should be noted that all three methods are very powerful, but each comes with its own set of advantages and disvantages that must be understood for its use.

Runge-Kutta methods propagate a solution over an interval by combining the information from several Euler-style steps (each involving one evaluation of the right-hand functions), and then using the information obtained to match a Taylor series expansion up to some higher order.

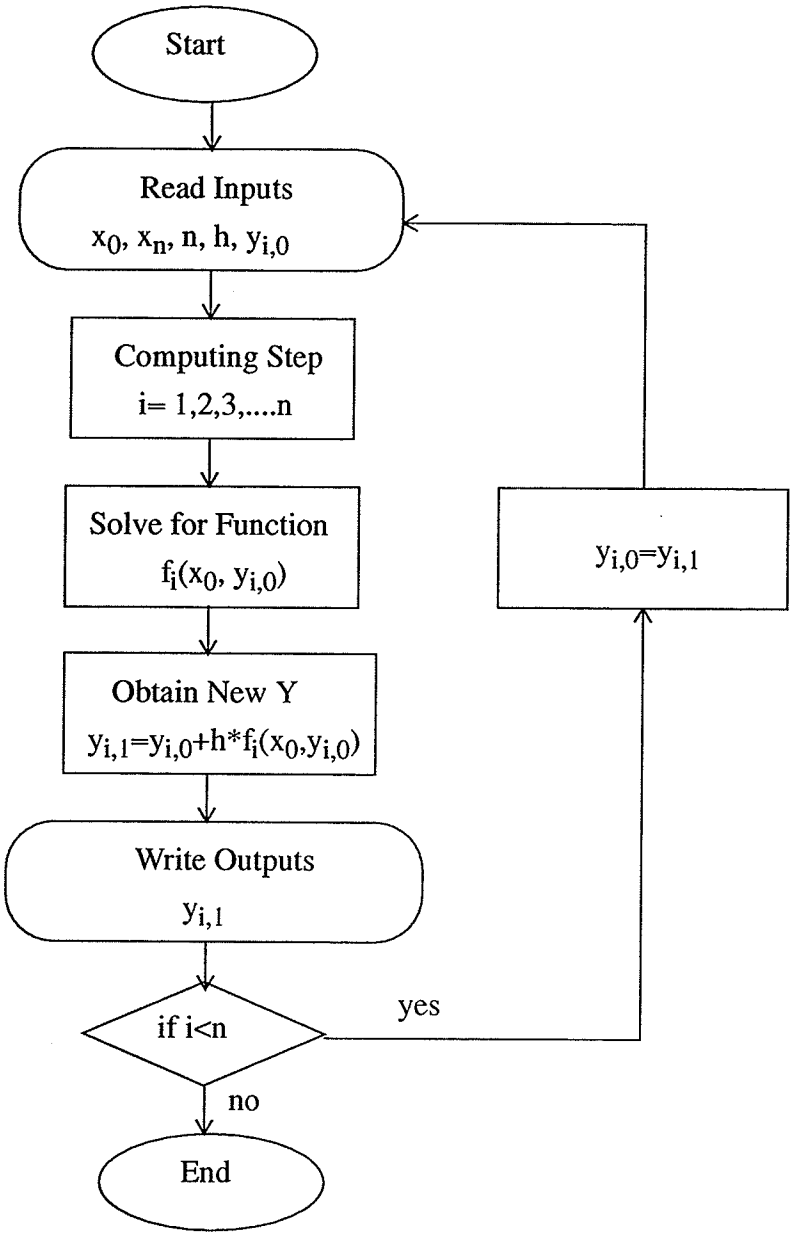

Fig. 3.1 Flow diagram of the algorithm

Richardson extrapolation uses the powerful idea of extrapolating a computed result to the value that would have been obtained if the stepsize had been very much smaller than it actually was. In particular, extrapolation to zero stepsize is the desired goal. When combined with a particular way of taking individual steps (the modified midpoint method) and a particular kind of extrapolation (rational function extrapolation), Richardson extrapolation produces the Bulirsch-Stoer method.

Predictor-corrector methods store the solution along the way, and use those results to extrapolate the solution one step advanced; they then correct the extrapolation using derivative information at the new point. These are best for very smooth functions.

Runge-Kutta is what people use when (a) they don't know any better, or (b) they have an intransigent problem where Bulirsch-Stoer is failing, or (c) they have a trivial problem where computational efficiency is of no concern. Runge-Kutta succeeds virtually always; but it is not usually fastest. Predictor-corrector methods, since they use past information, are somewhat more difficult to start up, but for many smooth problems, they are computationally more efficient than Runge-Kutta. Bulirsch-Stoer method is the best known way to obtain high-accuracy solutions to ordinary differential equations with minimal computational effort. However the method is not suitable for differential equations containing nonsmooth functions. For example, you might have a differential equation whose right-hand side involves a function which is evaluated by table look-up and

interpolation. If so, Runge-Kutta with adaptive stepsize choice is preferred. Furthermore the techniques in this Bulirsch-Stoer method are not particularly good for differential equations which have singular points inside the interval of integration. A regular solution must tiptoe very carefully across such points. Runge-Kutta with adaptive stepsize can sometimes effect this; more generally, there are special techniques available for such problems, beyond the scope here.

In general, for high-precision applications, or applications where evaluations of the right-hand sides are expensive, Bulirsch-Stoer dominates. For convenience, or for low-precision, adaptive-stepsize Runge-Kutta dominates. Predictor-corrector methods have been in the middle.

Since Runge-Kutta method is relatively simple and computational efficiency here is not of serious concern, the Runge-Kutta method was first chosen for our problem.

3.2.1 Runge-Kutta Method

The simplest numerical method is Euler's method. The formula for the Euler method is

$$y_{n+1} = y_n + hf(x_n, y_n) \tag{3.3}$$

which advances a solution from x_n to $x_{n+1} = x_n + h$. The derivation of Euler's method is very straightforward using the Taylor expansion of y about x which is

not given here. The formula is unsymmetrical: it advances the solution through an interval h, but uses derivative information only at the beginning of that interval (fig. 3.2). That means that the step's error is only one power of h smaller than the correction, i.e. $o(h^2)$ added to equation (3.3).

There are several reasons that Euler's method is not practical for use, among them, (a) the method is not very accurate when compared to other methods run at the equivalent stepsize, and (b) neither is it very stable.

Consider, however, the use of a step like equation (3.3) to take a "trial" step to the midpoint of the interval. Then use the value of both x and y at that midpoint to compute the "real" step across the whole interval. Figure 3.3 illustrates the idea. In equations,

$$k_1 = hf(x_n, y_n) \tag{3.4}$$

$$k_2 = hf(x_n + \tfrac{1}{2}h, y_n + \tfrac{1}{2}k_1) \tag{3.5}$$

$$y_{n+1} = y_n + k_2 + o(h^3) \tag{3.6}$$

As indicated in the error term, this symmetrization cancels out the first order error term, making the method second order (A method is conventionally called n^{th} order if its error term is $o(h^{n+1})$). In fact, equation (3.5) is called the second-order Runge-Kutta or midpoint method.

There are many ways to evaluate the right-hand side functions f(x, y) which all agree to first order, but which have different coefficients of higher-order

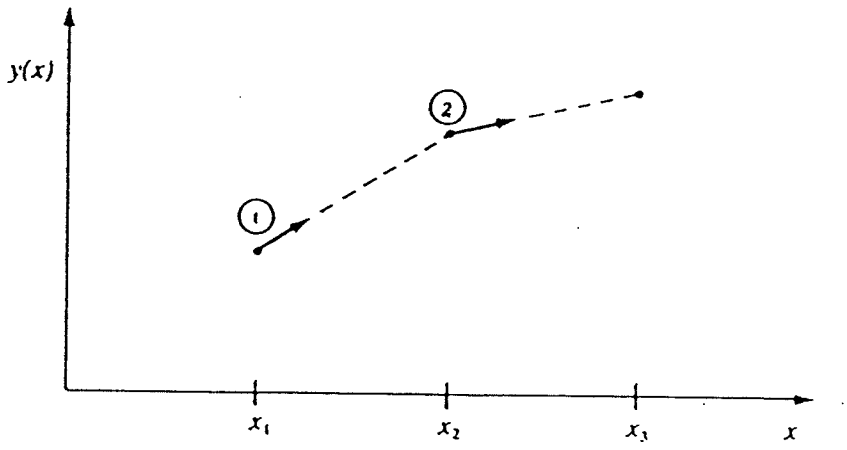

Fig.3.2 Euler's method. In this simplest (and least accurate) method for integrating an ODE, the derivative at starting point of each interval is extrapolated to find the next function value. The method has first-order accuracy (after W.H. Press et. al. [51]).

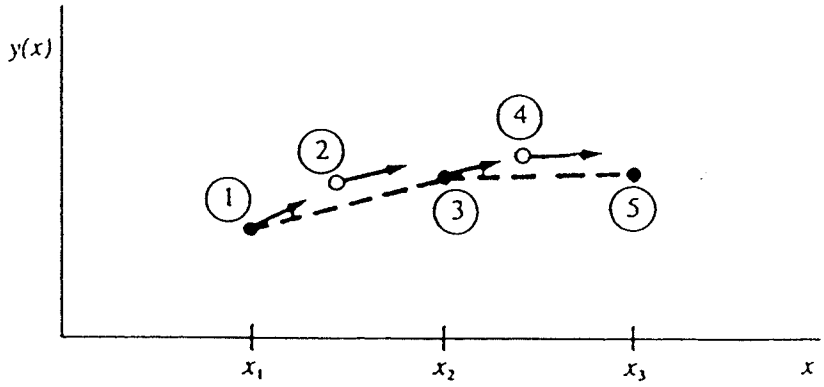

Fig.3.3 Midpoint method. Second order accuracy is obtained by using the initial derivative at each step to find a point halfway across the interval, then using the midpoint derivative across the full width of the interval. In the figure, filled dots represent final function values, while open dots represent function values that are discarded once their derivatives have been calculated and used (after W.H. Press et. al. [51]).

error terms. Adding up the right combination of these, we can eliminate the error terms order by order. That is the basic idea of the Runge-Kutta method. By far the most often used, and arguably even most useful, is the fourth-order Runge-Kutta formula, which has a certain sleekness of organization about it:

$$k_1 = hf(x_n, y_n) \tag{3.7}$$

$$k_2 = hf(x_n + \tfrac{1}{2}h, y_n + \tfrac{1}{2}k_1) \tag{3.8}$$

$$k_3 = hf(x_n + \tfrac{1}{2}h, y_n + \tfrac{1}{2}k_2) \tag{3.9}$$

$$k_4 = hf(x_n + h, y_n + k_3) \tag{3.10}$$

$$y_{n+1}=y_n+(k_1+2k_2+2k_3+k_4)/6+o(h^5) \tag{3.11}$$

The fourth-order Runge-Kutta method requires four evaluations of the right-hand side functions per step h (fig. 3.4). This will be superior to the midpoint method equation (3.4), in that at least twice as large a step is possible with equation (3.11) for the same accuracy. The fourth-order Runge-Kutta is generally superior to second-order, but high order does not always mean high accuracy. Actually for orders M higher than four, more than M function evaluations are required. That is why higher than fourth-order Runge-Kutta formulas are barely written down.

The Runge-Kutta method treats every step in a sequence of steps in identical manner. Prior behaviour of a solution is not used in its propagation. This is mathematically proper, since any point along the trajectory of an ordinary

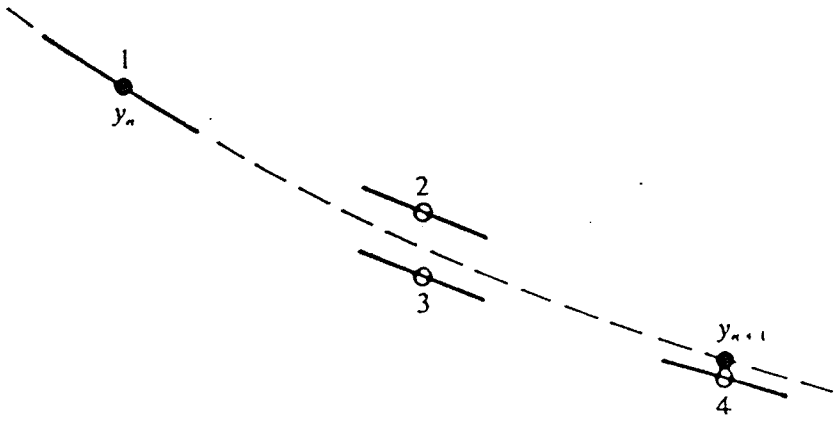

Fig.3.4 Fourth-order Runge-Kutta method. In each step the derivative is evaluated four times: once at the initial point, twice at trial midpoints, and once at a trial endpoint. From these derivatives the final function values (shown as a filled dot) is calculated (after W.H. Press et. al. [51]).

differential equation can serve as an initial point. The fact that all steps are treated identically also makes it easy to incorporate Runge-Kutta method into relatively simple computing routines.

From the derivation of formulae in chapter two, we can notice that many physical constants and parameters are involved in our problem. Some of these parameters, such as defect densities, sink strengths and vacancy concentrations in various sinks etc, are very sensitive to the temperature due to the exponential dependence. That is one of the important reasons that the calculation had been done in different temperature ranges.

We have chosen the Fourth order Runge-Kutta method to solve the system of ordinary differential equations (2.9) to (2.13). Several software packages for ODEs are available in general libraries such as IMSL, NAG and SL/MATH. But only the IMSL is supported by The University of Manitoba Computer Services [52]. One of the routines for ODEs, IVPRK, had been tried. Unfortunately it does not work out with the current problem owing to unidentified subroutines in its main program. On the other hand it is straightforward to write our own routine according to equations (3.7) to (3.11). Therefore a Fortran subroutine has been written incorporating equations (3.7) to (3.11).

Since the written subroutine is non-tested, it is necessary to verify it by applying it to a problem to which the solution is known. Consider a famous predator-prey problem with rabbits and foxes [52]. Let r be the density of rabbits and let f be the density of foxes. In the absence of any predator-prey interaction

the rabbits would increase at a rate proportional to their number, and the foxes would die of starvation at a rate proportional to their number. Mathematically,

$$r' = 2r$$

$$f' = -f.$$

The rate at which the rabbits are eaten by the foxes is 2rf and the rate at which the foxes increase, because they are eating the rabbits, is rf. So the system to be solved is

$$r' = 2r - 2rf$$

$$f' = -f + rf.$$

The initial conditions are r(0)=1 and f(0)=3 over interval $0 \leq t \leq 10$. In the following program Y(1)=r and Y(2)=f.

PROGRAM

```
C
      DIMENSION Y(2),YT(2),DYT(2),DYM(2),DYDT(2)
      OPEN (UNIT=44,FILE='dat.507')
C                                     initial conditions
      GDPA=0.E0
      Y(1)=1.E0
      Y(2)=3.E0
C                                     integration loop
      DO 5 I=1,100
      H=1.E-1
      HH=H*0.5E0
      H6=H/6.E0
C                                     initialize rk-method
      CALL FUNCT(Y,DYDT)
      DO 10 J=1,2
      YT(J)=Y(J)+HH*DYDT(J)
10    CONTINUE
```

```
      CALL FUNCT(YT,DYT)
      DO 20 K=1,2
      YT(K)=Y(K)+HH*DYT(K)
20    CONTINUE
      CALL FUNCT(YT,DYM)
      DO 22 M=1,2
      YT(M)=Y(M)+H*DYM(M)
      DYM(M)=DYT(M)+DYM(M)
22    CONTINUE
      CALL FUNCT(YT,DYT)
      DO 24 N=1,2
      Y(N)=Y(N)+H6*(DYDT(N)+DYT(N)+2*DYM(N))
24    CONTINUE
      GDPA=GDPA+H
      WRITE(44,'(E10.2,2E11.4)')GDPA,(Y(K),K=1,2)
5     CONTINUE
      STOP
      END
C
      SUBROUTINE FUNCT(Y,DYDT)
      DIMENSION Y(2),DYDT(2)
      DYDT(1)=2.E0*Y(1)-2.E0*Y(1)*Y(2)
      DYDT(2)=Y(1)*Y(2)-Y(2)
      RETURN
      END
```

The output of the program is listed as follow,

Output

Time	Y(1)	Y(2)
1.000	0.077	1.464
2.000	0.085	0.578
3.000	0.291	0.249
4.000	1.447	0.187
5.000	4.051	1.440
6.000	0.176	2.258

7.000	0.065	0.909
8.000	0.147	0.367
9.000	0.651	0.188
10.00	3.146	0.349

The following plots (figs. 3.5, 3.6) are the results of calculated output. The results are consistent with the solution calculated through a different routine in the IMSL.

Having finished the verification of the written subroutine, we are able to apply its scheme into the present problem with appropriate choice of physical constants and parameters. The computed results are consistent with the steady-state solution in published works [37,43].

However, it is desirable that a different numerical method be used to double check the solution, as another test for the present computer program. Furthermore, the Runge-Kutta method only works well using very small stepsize h, as low as 10^{-5} order, and involves a long running time. For practical purposes, the irradiation dose has to be calculated up to 30 to 50 dpa. This in turn requires (3 to 5)$\times 10^{6}$ evaluations of the right-hand side functions in equations (2.9) to (2.13). Theoretically, the more the amount of computing, the more the rounding error is, although the requirement of computing accuracy is not high (one of the reasons that a double precision is not used in the program). Also Computer Services only allocates limited data storage space (<15 megabytes) in the open area for each user.

3.2.2 The Method for Stiff Equations

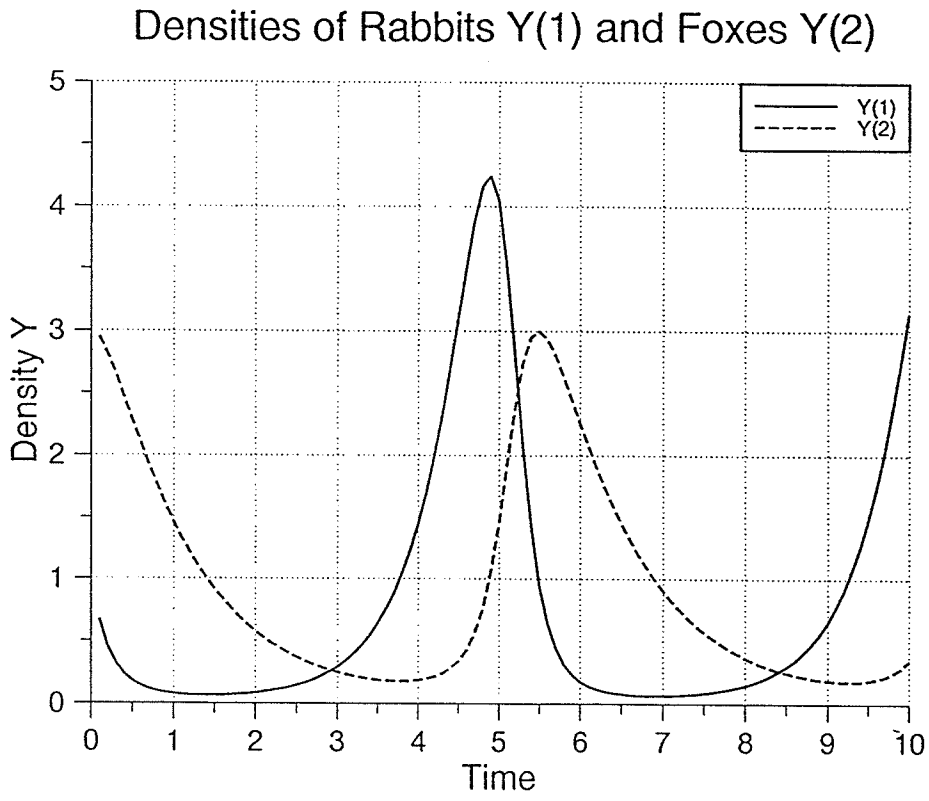

Fig.3.5 Time dependence of the densities of rabbits and foxes in the predator-prey problem.

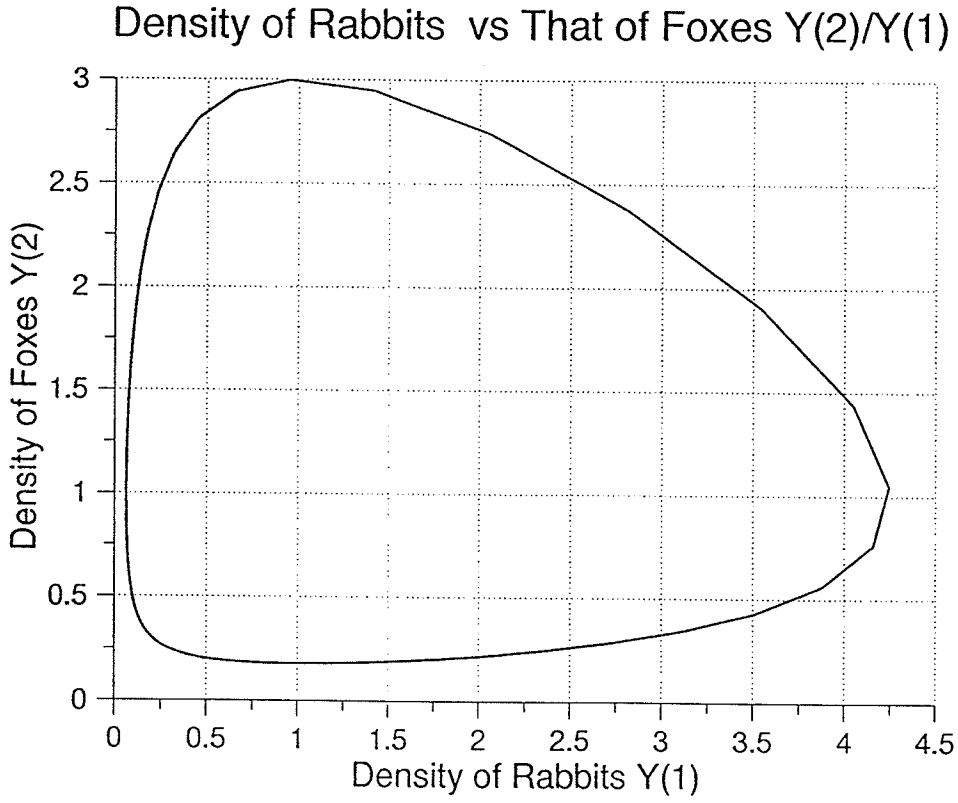

Fig.3.6 The phase diagram for the predator-prey problem of rabbits and foxes.

There are several technical definitions of **stiff** for a system of differential equations [50,53,54]; each is an attempt to mathematically describe a fairly common class of difficult problems. An intuitive description of stiffness is that the system has some solutions that change very rapidly compared with other solutions, or some solutions change very rapidly sometimes and slowly at other times. Physical processes, such as chemical reactions proceeding to equilibrium and discharging capacitors, that have a transient behaviour and a very stable steady state are often stiff. In the present problem, equations (2.9) to (2.12), for the densities of defect clusters and the defect contents in defect clusters, behave much differently from the equation (2.13) for void swelling, and from previous studies we found that the defect densities are of the order of 10^{23}, while void swelling is of the order of 10^{-1}. Also the fact that a stiff problem seems to be unstable, and the usual numerical methods require a very large number of steps to achieve even a modest accuracy, suggests that our problem to be stiff.

There is an available numerical scheme for stiff equations which removes or at least reduces the stiffness [51] could be adopted. For equation (3.1), an implicit method which can be constructed,

$$Y_{n+1}=Y_n+\tfrac{1}{2}h[f(x_{n+1},Y_n)+(\partial f/\partial Y)\big|_{Y_n}(Y_{n+1}-Y_n)+f(x_n,Y_n)] \qquad (3.12)$$

where Y_n is a vector. To solve for Y_{n+1}, the Jacobian matrix $(\partial f/\partial Y)\big|_{Y_n}$ must be inverted at each step. This is very expensive. Alternatively, the system of

equations (2.10) to (2.12) can be rewritten in a general form,

$$Y_{n+1} = f(x_n, Y_n) = \alpha - Y_n g(x_n, Y_n) \tag{3.13}$$

from which

$$\partial f/\partial Y|_{Yn} = -g(x_n, Y_n) - Y_n(\partial g/\partial Y)|_{Yn} \tag{3.14}$$

If the stepsize $h=x_{n+1}-x_n$ is chosen to be very small, the difference between $f(x_{n+1}, Y_n)$ and $f(x_n, Y_n)$ is negligible. Inserting equation (3.14) into equation (3.12), Y_{n+1} can be expressed as,

$$\begin{aligned} Y_{n+1} &= Y_n + h[f(Y_n) + \tfrac{1}{2}(\partial f/\partial Y)|_{Yn}(Y_{n+1}-Y_n)] \\ &= Y_n + h\{\alpha - Y_n g(Y_n) - \tfrac{1}{2}[g(Y_n) + Y_n(\partial g/\partial Y)|_{Yn}](Y_{n+1}-Y_n)\} \\ &= Y_n + h[\alpha - \tfrac{1}{2}(Y_{n+1}+Y_n)g(Y_n) - \tfrac{1}{2}Y_n(\partial g/\partial Y)|_{Yn}(Y_{n+1}-Y_n)] \end{aligned}$$

Now a further approximation $Y_n \approx \tfrac{1}{2}(Y_{n+1}+Y_n)$ in the third term in the square bracket is made because the change in consecutive Y is slight when stepsize h is chosen to be very small. Then

$$\begin{aligned} Y_{n+1} &= Y_n + h\{\alpha - \tfrac{1}{2}(Y_{n+1}+Y_n)[g(Y_n) + \tfrac{1}{2}(\partial g/\partial Y)|_{Yn}(Y_{n+1}-Y_n)]\} \\ &= Y_n + h[\alpha - \tfrac{1}{2}(Y_{n+1}+Y_n)g(Y_{n+\frac{1}{2}})]. \end{aligned}$$

Therefore

$$Y_{n+1} = \{\alpha h+[1-\tfrac{1}{2}hg(Y_{n+\frac{1}{2}})]Y_n\}/[1+\tfrac{1}{2}hg(Y_{n+\frac{1}{2}})]. \quad (3.15)$$

Similarly

$$Y_{n+\frac{1}{2}} = \{\tfrac{1}{2}\alpha h+[1-\tfrac{1}{4}hg(Y_n)]Y_n\}/[1+\tfrac{1}{4}hg(Y_n)]. \quad (3.16)$$

The equations (3.15) and (3.16) have become the modified formulae for the method for stiff equations. They avoid the complex evaluation of the Jacobian matrix. Of course, we give up some accuracy by performing the above approximation, but the resulting error is under the error tolerance due to moderate precision requirement in our problem. From the computation it is found that this scheme reduced the stiffness in the equations, but did not remove it completely. The stepsize can be chosen at range $\leq 10^{-4}$ which is one order larger that the one ($\leq 10^{-5}$) in the Runge-Kutta method. So the amount of computation is ten times less, and the effort to handle the output data generated from computing is also reduced to a reasonable load. The results calculated from this method are in accord with the ones from Runge-Kutta method.

CHAPTER 4

RESULTS AND DISCUSSION

4.1 Material and Irradiation Parameters

For the purpose of this research, fast neutron irradiation with 316 stainless steel is considered. Austenitic stainless steel, which is an alloy of chromium, nickel and iron, possesses a faced-centred-cubic structure. The reason the work focuses on austenitic stainless steel and irradiation by neutrons is that the steel is a commercially important alloy and is widely used in fast breeder reactors. It is also one of the materials proposed for use in future DT fusion reactors. The neutrons are the product of two of four energy sources which have been identified as offering the potential for an "indefinitely sustainable" energy supply [56] -- nuclear fission with breeding and controlled thermonuclear fusion of deuterium and tritium (DT). The material and irradiation parameters used as input parameters in our computation are listed in table 4.1 and come from published works in the literature [30,37,57,58].

There are at least two general goals in developing models such as have been described in Chapters 1 and 2 [58]. One is to try to develop an understanding of the important physical processes involved in the evolution of the microstructure under irradiation, and the other is to ultimately provide some predictive capability. The satisfaction of both of these goals is frustrated by a lack of information on important material parameters for austenitic stainless steel. In some cases, measurements made on pure metals can be used to provide initial estimates, but key parameters are sometimes sensitive to alloy composition and perhaps impurities [59-64]. Simple void swelling models have been successfully used to explain much of the available swelling data and have provided considerable insight into the mechanisms responsible for this phenomenon [65,66]. However, the ability to do predictive work with these models is compromised by uncertainty about parameter values. For instance, when bulk recombination is ignored and dislocations are the major point defect sink, the vacancy supersaturation takes the following simple form [67],

$$S = \frac{\eta G_{dpa}}{S_i^n D_v C_v^e} (Z_i^n - 1) \qquad (4.1)$$

Values of the cascade efficiency η between 0.1 and 1.0 and dislocation bias Z_i^n between ~1.02 to >1.5 have been used by various workers. Depending on the values chosen for the two parameters, the computed supersaturation can vary significantly.

Table 4.1 Material and irradiation parameters.

parameter	Value
Jump distances b for vacancies and interstitials[1]	2.53×10^{-10} m
Atomic volume[3]	1.15×10^{-29} m^3
Dislocation bias[2] p	0.3
Dislocation bias factor for vacancies[2] Z	2.0
Vacancy migration energy[3]	1.4 eV
Vacancy formation energy[3]	1.6 eV
Vacancy diffusitivity pre-exponential[3]	8×10^{-5} m^2s^{-1}
Average loop-line energy[4] ΔE	0.3 eV
Surface free energy[3] γ	$(3.24\text{-}1.4)\times10^{-3}T(^0C)$ Jm^{-2}
Total interstitial loop density[3] N_{il}	$5\times10^{27}\exp[-0.0327T(^0C)]$ m^{-3}
Total network dislocation density[3] ρ_N	$6.8\times10^{16}\exp[-0.0096T(^0C)]$ m^{-2}
Total void number density[3] N_c	$2.53\times10^{26}\exp[-0.023T(^0C)]$ m^{-3}
Total void strength[1] k_c^2	$(4\pi N_c)^{2/3}(3S)^{1/3}$; S=10%
Total interstitial loop sink strength[1] k_{il}^2	$N_{il}(\pi/\rho)^{1/2}Z$
Intercascade interstitial clustering fraction[1] ε_i	0.45
Intercascade vacancy clustering fraction[1] ε_v	0.5
Average initial radius of PICs[1] r_{i0}	2b
Average initial radius of PVCs[1] r_{v0}	3b
Average initial radius of voids r_{c0}	10×10^{-10} m
(NRT) d.p.a. rate[1] K	10^{-6}d.p.a.s^{-1}
Effective point-defect generation rate[1] G	10^{-7}d.p.a.s^{-1}

1. Data from Woo and Semenov (1993).
2. Data from Skinner and Woo (1984).
3. Data from Stoller and Odette (1987).
4. Data from Foreman and Makin (1979).

A partial list of these uncertain parameters would include material properties such as the activation energy for self-diffusion, the matrix surface free energy and dislocation bias, and irradiation parameters such as the cascade efficiency. In many cases, these parameters have been measured in either pure materials or simple alloys and the values have been applied to complex alloys. The influence of alloy composition is either ignored or extrapolated from measurements at a few compositions. In other cases no direct measurements are available and values are inferred from indirect observations. Even in the best of cases, experimental uncertainties typically lead to a large enough range of "reasonable" values for any given parameter that model predictions can be significantly affected. Finally, the use of theory fitting to experiments to help define the range of parameter values is also difficult because changes in one parameter is often offset by a corresponding change in another. For example, changes in the cascade efficiency in equation (4.1) can be directly offset by changes in the bias or the dislocation density. One of the advantages of the present model as discussed in chapter two is that simple relations such as equation (4.1) do not arise from the explicit dose and temperature dependence of the major microstructural sinks. However, even in the comprehensive model, some limited parameter variations could be offset by changes in other parameters. However, the result of the uncertainties is that it is generally impossible to arrive at a unique set of model parameters by fitting the theory to observations in any one data set. Therefore, with even a well-calibrated model, any extrapolation from the existing

data base should be carried out with great care.

A few of examples in which the choice of parameter values used in the present work is discussed are presented below [68]. Experiments to measure the self-diffusion coefficient in austenitic alloys are typically conducted at quite high temperatures (T = 1000 to 1400^0 C) [61,62,69]. Extrapolation of these results to temperatures in the range 300 to 700^0 C is uncertain since relatively small changes in the activation energy will lead to large errors at these lower temperatures. The value of the activation energy is known to be sensitive to composition [70] and typical values range from ~2.6 to 3.2 eV in various austenitic alloys [61,62,71,72]. An intermediate value of 3.0 eV can be used with a pre-exponential of 8.0×10^{-5} m^2 sec^{-1} [69,72]. The partitioning of the activation energy for self-diffusion between the vacancy formation and migration energies influences the results of the present model primarily for temperatures greater than about 600 to 650^0 C. Garner and Wolfer [73] have cited measurements of E^f_v which indicate that E^f_v ~ 1.8 eV and E^m_v ~ 1.1 eV in nickel and suggested that these values be used for type 316 stainless steel. However, measurements of E^m_v in both high purity Fe-Cr-Ni austenitic alloys and in type 316 stainless steel indicate that E^m_v ~ 1.3 to 1.4 eV; hence E^f_v ~ 1.5 to 1.6 eV. These latter values are more appropriate and for the present study values of E^m_v = 1.4 eV and E^f_v = 1.6 eV have been used.

Only a very limited number of measurements exist for the surface free energy in austenitic steels [63,74]. Murr and co-workers have reported measurements in type 304 stainless steel obtained using the method of zero creep

deformation of thin wires at high temperatures [74]. A linear fit to their data in the range of 1000 to 1400^0 C yields the following expression,

$$\gamma(T) = 4.05 - 1.75 \times 10^{-3}\ T(^0C)\ J/m^2 \qquad (4.2)$$

This leads to values of the surface energy between 2.8 and 3.5 J/m^2 when extrapolated to the 300 to 700^0 C temperature range. This is much higher than the nominal 1.0 J/m^2 which has typically been used in previous studies of void swelling. A lower surface energy can be rationalized on the basis of the presence of surface-active gases such as oxygen, but the amount of reduction which should be applied is unclear. This is particularly true in complex alloys where the presence of oxygen-gathering elements such as carbon, silicon and titanium appears to strongly limit the influence of oxygen. The 1.0 J/m^2 value has been used in the past largely because such a low value was required to obtain reasonable void nucleation rates from the classical stochastic theory. The value we used here retains the temperature dependence of equation (4.2), but the magnitude is reduced by a factor of 0.8. The change reflects better agreement with the values measured in austenitic alloys.

A critical discussion of every parameter is beyond the scope of this thesis. The values of parameters used in the work have been carefully chosen and calibrated to reflect the real irradiation environment. It should be emphasized that the specific values of the predicted swelling are sensitive to model assumptions

and parameters. However, the general trends which are predicted are a consequence of the physical mechanisms and not the details of the model parameters.

The computer program written in Fortran solving the system of differential equations is listed in appendix A, and the input and output parameters are tabulated in appendix B and C. A typical output data set is also included in appendix D.

4.2 Defect Cluster Evolution and Void Swelling

Although the evolution of defect cluster distribution and the swelling of voids have been calculated from the equations (2.9)-(2.13) only under a set of rather simple assumptions, some general trends can be outlined.

Generally, at all temperatures concerned, the densities and the sizes of primary defect clusters go through a rapid increase in the early irradiation stage, and then start to saturate even at doses as low as 10^{-3} to 10^{-2} dpa. After which the constant trends are maintained to very high doses (figs. 4.1 to 4.3). Void swelling increases rapidly as long as cascade irradiation is present (figs. 4.4 to 4.7).

In order to model the evolution of defect clusters, the densities and sizes of PICs and PVCs as a function of irradiation dose are calculated according to eqs. 2.10 to 2.13. The calculated results are plotted in figs. 4.1 to 4.3 at different temperatures. In all figs. 4.1 to 4.7, the unit for irradiation dose is NRT dpa

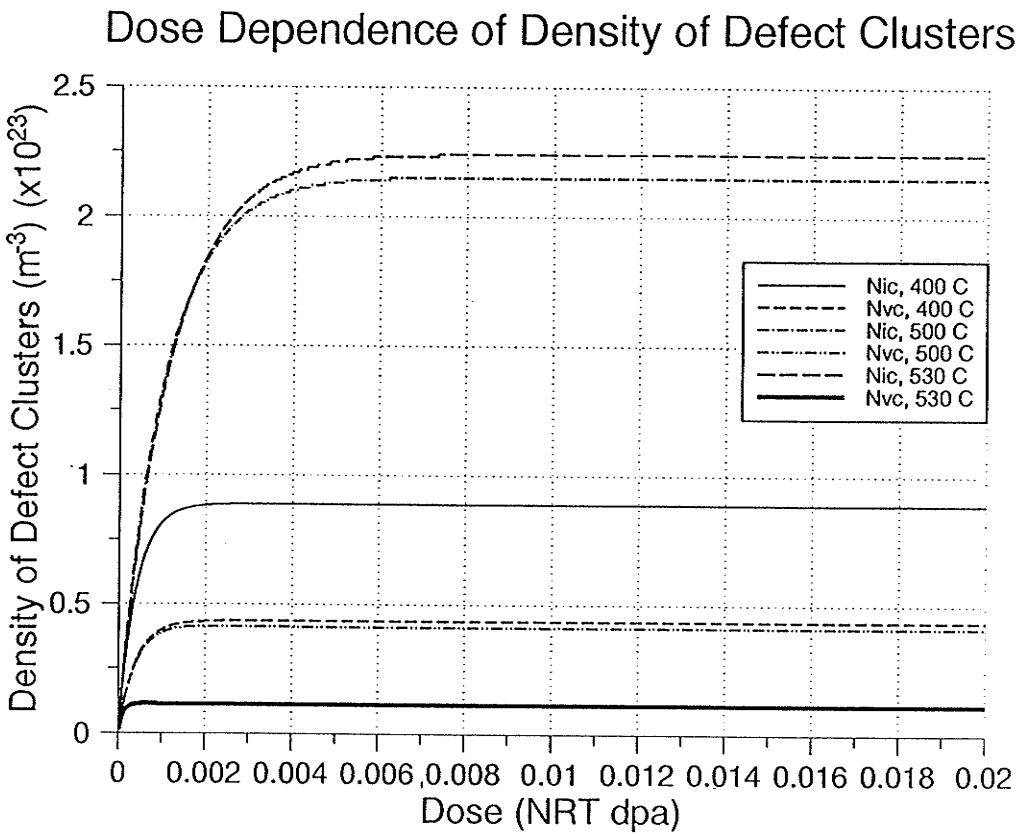

Fig.4.1 Dose dependence of calculated number densities of the PICs and PVCs for 316 stainless steel in different temperature regions: low swelling (400°C), swelling peak (500°C) and post swelling-peak(vacancy evaporation from voids) (530°C). The material parameters are listed in the appendix B.

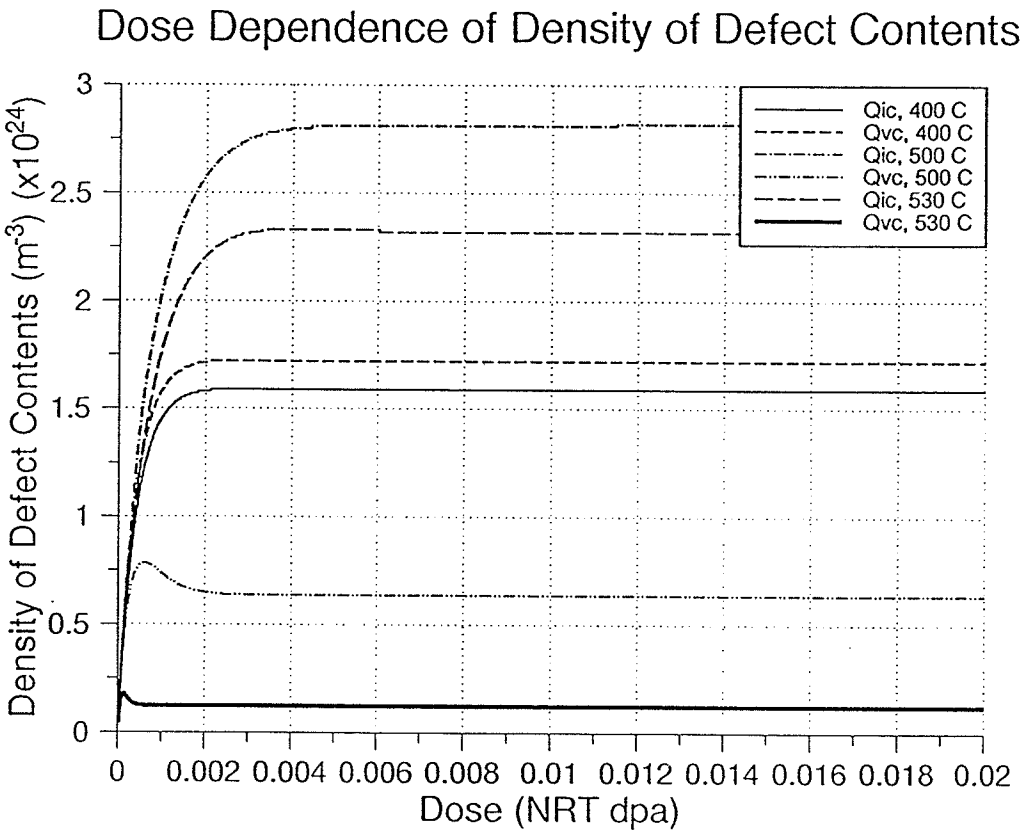

Fig.4.2 Dose dependence of calculated average total defect contents in the PICs and PVCs for 316 stainless steel in different temperature regions: low swelling (400°C), swelling peak (500°C) and post swelling-peak (vacancy evaporation from voids) (530°C). The material parameters are listed in the appendix B.

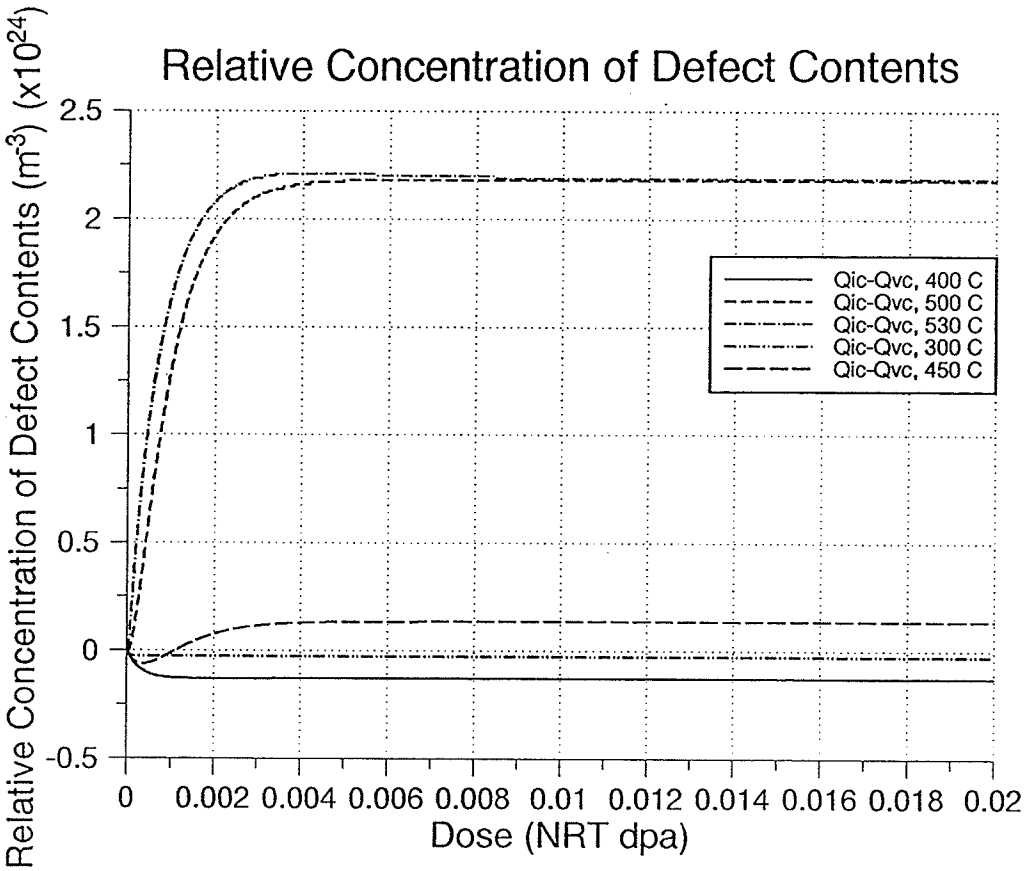

Fig. 4.3 Dose dependence of calculated difference between interstitial concentration in PICs and vacancy concentration in PVCs. Parameters are the same as the ones used to derive figs. 4.1 and 4.2.

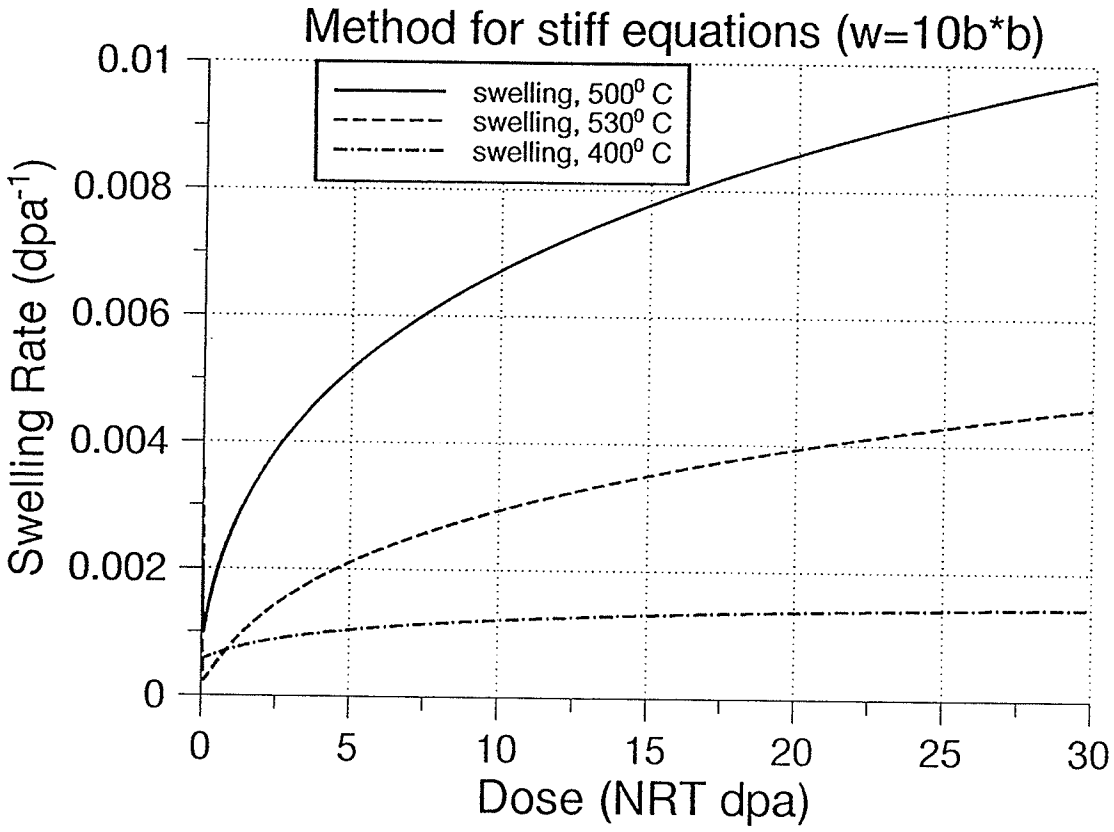

Fig.4.4 Dose dependence of calculated void swelling rate for 316 stainless steel in different temperature regions: low swelling (400°C), swelling peak (500°C) and post swelling-peak(vacancy evaporation from voids) (530°C). The material parameters are listed in the appendix B.

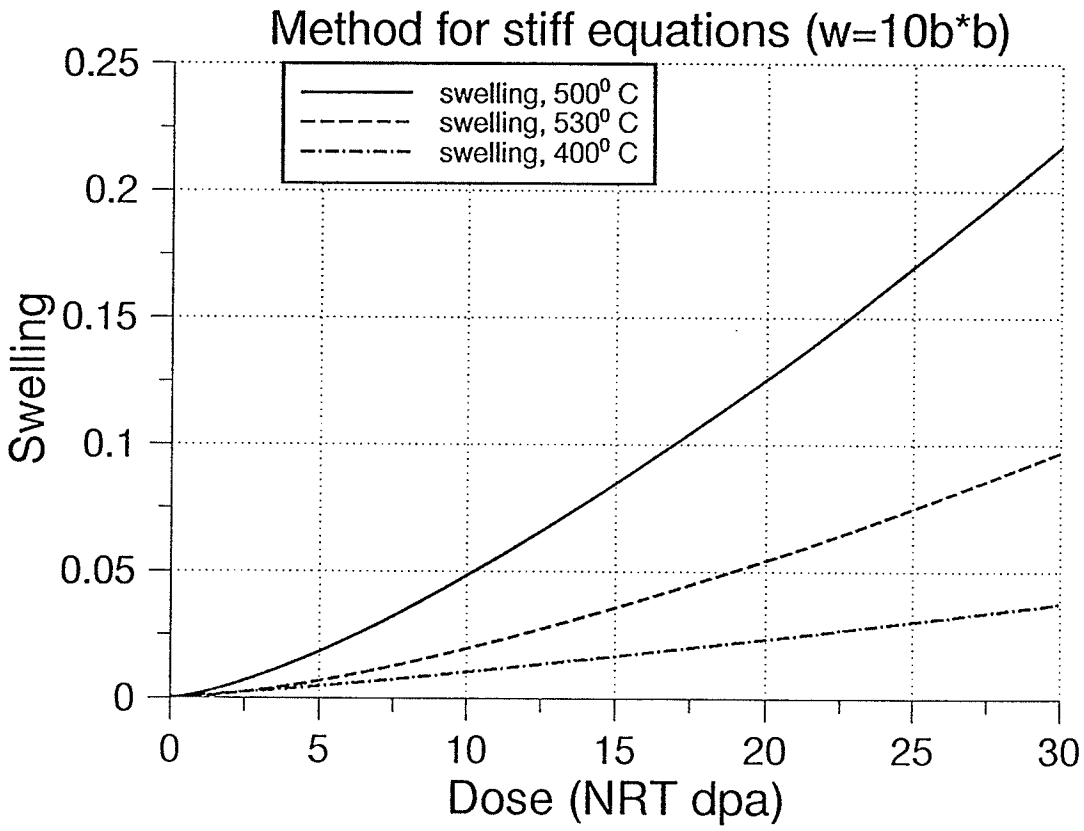

Fig.4.5 Dose dependence of calculated void swelling for 316 stainless steel in different temperature regions: low swelling (400°C), swelling peak (500°C) and post swelling-peak(vacancy evaporation from voids) (530°C). The material parameters are listed in the appendix B.

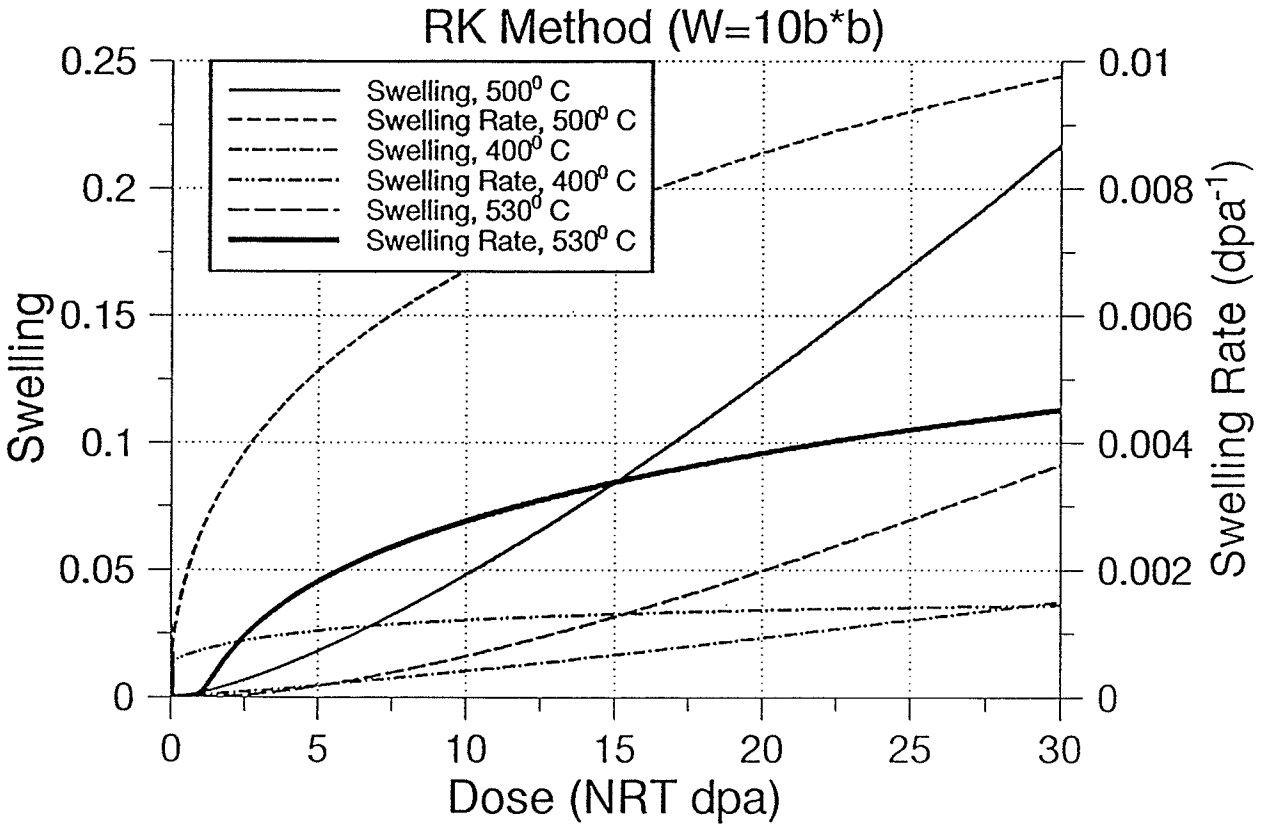

Fig.4.6 Dose dependence of calculated void swelling using Runge-Kutta method. Parameters are the same as the ones used to derive figures 4.4 and 4.5.

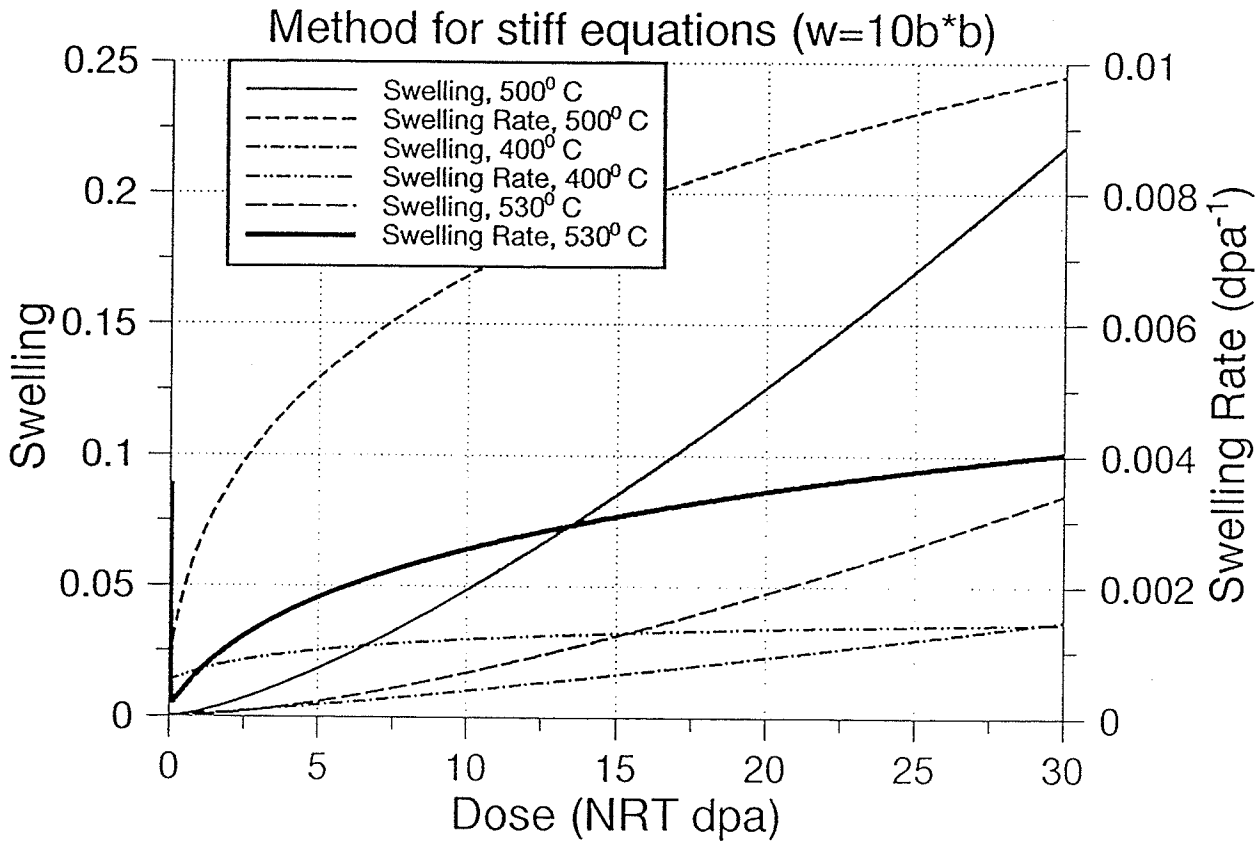

Fig.4.7 Dose dependence of calculated void swelling using the method for stiff set of equations. Parameters are the same as the ones used to derive figures 4.4 and 4.5.

(displacement per atom). In fig. 4.1 the unit for densities is m^{-3} (numbers of PICs or PVCs per atomic volume). In figs. 4.2 and 4.3 the unit for defect content is m^{-3} (numbers of vacancies or interstitials per atomic volume in PICs or PVCs respectively). The calculated void swelling rate according to equation (2.9) is shown in figs. 4.4 to 4.7 as a function of irradiation dose at three different temperatures. In fig. 4.4 the unit for void swelling rate is the mean volume strain of voids per dpa. In fig. 4.5 the unit for void swelling is the mean volume strain of voids. The dose has been calculated up to 30 dpa. The specific temperatures 400°C, 500°C and 530°C in the figs are chosen to reflect the variation of void swelling with temperature, in the low swelling, peak swelling and post peak-swelling (vacancy evaporation from voids) temperature regions respectively. The figs. 4.6 and 4.7 are the calculated results using Runge-Kutta method and the method for stiff equations. It is evident that the different methods have generated the same result of void swelling.

At low temperatures, such as 400^0 C, at which the thermal evaporation of vacancies from all vacancy clusters is unimportant, and the dislocation density is high; the dislocation bias is mostly predominant. After extensive bulk recombination and segregated defect clustering of like type, only very small fraction of point defects survive as mobile defects. A great number of mobile interstitials and vacancies and their clusters annihilate in the sinks such as dislocation loops and network dislocations by absorption, due to high dislocation concentration. Therefore, the steady-state concentrations of defect clusters are

low, as illustrated in figs. 4.1 and 4.2. Since the dislocation bias has a preferential attraction for interstitials, more interstitials than vacancies are annihilated at dislocations. This produces a small net vacancy flux which contributes to the defect accumulation in sinks such as voids. No significant void swelling occurs because of the small vacancy flux, as shown in figs. 4.4 to 4.7.

At elevated temperatures, such as 500^0 C, PVCs become thermally unstable whereas PICs are still stable due to the higher binding energy [75]. For example, MD calculations have found that the binding energy of a tetra-interstitial cluster in copper is 2.53 eV, whereas the binding energy for a tetra-vacancy cluster is only 0.28 eV; the corresponding binding energy per defect for clusters containing more than 5 point defects is ~0.85 eV/interstitial and ~0.44 eV/vacancy, respectively [76,77]. Even larger differences between the stability of small vacancy and interstitial clusters have been obtained for nickel [77]. As noted by Simons [78] and Woo and Singh [26,27], this difference in stability between vacancy and interstitial clusters leads to an excess supply of mobile vacancies relative to the mobile interstitial population at elevated temperatures.

The thermal vacancy evaporation from vacancy clusters results in a substantial net vacancy flux to the medium since the portion of point defects immobilized in clusters can be an order of magnitude greater than that of survived mobile point defects in cascades. Vacancy evaporation has been reflected by large reduction both of the density of PVCs and of the vacancy content in PVCs at temperature 500^0 C in figs. 4.1 and 4.2 respectively. Meanwhile, as the temperature increases,

the dislocation density decreases. Therefore, fewer PICs are lost in dislocations by absorption. The high density and interstitial content of PICs can be noticed in the graph. It is plausible that the more numerous atomic displacements at elevated temperatures also contribute to the high density of PICs at 500^0 C. Actually, the interstitials in PICs are only the balance of annihilation between the PICs and a portion of evaporating vacancies. A substantial amount of evaporated vacancy flux adds the vacancy supersaturation in voids except diffusing into other sinks (e.g. dislocations, loops and PICs etc.). This is the reason that a much higher swelling rate occurs at elevated temperature regime as shown in figs. 4.4 and 4.5. Based on such biased vacancy supply or consideration of two types of defect clustering in cascades, Woo and Singh [26,27] have developed the theory of production bias as a potent driving force for high swelling rates at elevated temperatures. The production bias incorporated in the new model predicts very well the experimental observation of swelling in structural materials, while conventional mean field theory using dislocation bias as a sole driving force fails to do. In fact at elevated temperatures the effect of dislocation bias still exists, but is relatively insignificant. The production bias is predominant, and PVCs act as an internal source of mobile defects, in contrast to the cascades as an external source.

As the irradiation continues, more point defects are generated. Therefore the primary cluster concentrations increase proportionally with respect to irradiation dose at the early stage of irradiation as shown in figs. 4.1 and 4.2.

However, a quasi-steady state is soon reached, at which the concentrations of clusters actually keep a dynamic equilibrium between creation and annihilation. It is clear that point defects and their clusters are continually produced in cascades. Through absorption at dislocations, biased absorption of interstitials and evaporation of vacancy clusters, cascade-induced PVCs are removed. From the graph, the dynamic equilibrium of PICs also persists, but the mechanism of removing PICs is not very straightforward and is coupled with different processes.

Foreman and Makin [30] suggested five processes of annihilation of stable PVCs in the form of small vacancy loops in which two have been extended for the removal of PICs by Woo, Semenov and Singh [37, 43]: 1) dislocation sweeping, and 2) glide of some primary clusters (as small dislocation loops) and their coalescence. Woo and Semenov [37] modeled the reaction between the primary clusters and the dislocations (i.e. loops and network) by assuming that the primary clusters have the form of immobile small dislocation loops. These loops are formed in cascades, or by coalescence near the cascade volume where the density of the primary clusters is highest, or when trapped, after long-range glide, in the strain fields of dislocations. The absorption of the PICs by the dislocations was then described in terms of a dislocation sweeping model in which the absorption process at the dislocation core is assumed to be the rate controlling process. Trankaus, Singh and Foreman [79] also investigated the annihilation of PICs by one-dimensional glide in the presence of voids and dislocations. They suggested that the small glissile PICs are preferentially annihilated at extended

sinks such as dislocations and grain boundaries. The removal of the PICs yields an excess of vacancies which may induce the void swelling. In particular, the high swelling rate of well annealed metals with negligible dislocation density at low doses [79] and the enhanced swelling rate observed in regions adjacent to grain boundaries can be attributed to the escape of PICs to these planar sinks.

Kroupa [80] studied the interaction between prismatic loops and straight dislocations, and found that the interaction can be either attractive or repulsive depending on the relative orientations, and reach a maximum in most cases when the loops and the dislocations touch. In perspective, such an interaction can be an order of magnitude larger than that between substitutional impurities and dislocations (usually considered in theories of solution hardening [81]). This is because the interaction is proportional to the volume of the loop, $\pi r_l^2 b$, which is large compared to the value of a fraction of an atomic volume for the case of substitutional atoms. In the presence of attractive obstacles , a dislocation at zero stress attains the minimum energy in a zigzag configuration in the glide plane, with points at which the dislocation is pinned by the obstacles [82,83]. Therefore, when one or more of the pinning clusters are annihilated by absorption at its core, or when a nearby vacancy cluster evaporates, the dislocation segment becomes unstable in the field of primary clusters, and glides towards a new minimum energy configuration, to be pinned again by other primary clusters on its way, and the whole process starts all over again. In fact, the glide towards a new minimum energy configuration is very much facilitated by the climb of the dislocation due

to absorption of point defects, either freely migrating or bound in the primary clusters.

During fast neutron irradiation, overlaping cascades may interact by impingement. Cascade impingement can destroy newly established PICs which are small and unstable compared to other sinks in the matrix. Thus cascade impingement also plays a role in the annihilation of PICs.

From foregoing discussion, it is suggested that PVCs and PICs have a different annealing behaviour. Due to fast vacancy evaporation, PVCs shrink and even vanish. The evaporated vacancies diffuse into the medium, and contribute to the vacancy accumulation in voids. Voids are basically immobile, and only grow in size. PICs join dislocations in groups by glide whereas dislocations climb and glide and sweep up PICs. The evaporating vacancies can recombine at PICs and suppress the build-up of PICs as the cascade impingement does.

The reason, that a cut-off appears in the curve of swelling rate at zero dose in the figs. 4.4 to 4.7, is that a non-zero average initial radius of voids is set. Such a simplification is necessary since the subject of void nucleation is beyond the scope of the present thesis.

At high temperatures, such as 530°C and above, the voids become thermally unstable because the vacancies in them start evaporating, owing to the surface tension of voids. Therefore, the swelling rates become lower (figs. 4.4 to 4.7) as evaporating vacancies from voids offset the flux of diffusing vacancies in the matrix. If the gas pressure in voids were taken into account, the thermal

instability of the voids would start at a higher temperature, and it is speculated that the swelling rates will drop much slower.

In neutron irradiation environments, helium and hydrogen are produced in structural alloys through (n,α) and (n,p) transmutation reactions respectively. The exact quantities produced depend upon the composition of the material and the neutron energy spectrum. In the fusion environment, the high gas production rates in steels may influence the microstructural response of the material, particularly at higher temperatures. While the role of hydrogen as a fast diffuser is not unambiguously determined, helium has been assumed by many researchers to play a key role in assisting void nucleation from the time that Cawthorne and Fulton first observed void swelling [1]. Some authors have discussed the results of neutron (with helium either preinjected or simultaneously injected with the damage producing ions) irradiation experiments in which the total void density appears to increase with the helium content. In some cases the dependence of the void density on the helium concentration could crudely be described by a simple power law [84]. Singh and Foreman [85] have also investigated the influence of helium on void formation and found similar results. They note that the void density is roughly proportional to the square root of the helium generation as mentioned above. Even though the role of gases, in particular helium, is complex and is another subject in the neutron irradiation, it is desirable that a model incorporating the effects of gases at high temperatures be developed in further studies, because the void swelling becomes sensitive to another irradiation parameter; namely the

transmutation gas generation rate at temperatures above about 525^0 C in reactors [28].

CHAPTER 5

SUMMARY

While considering the accumulation of defects under cascade irradiation conditions, it is important to note that only a small fraction of NRT displacements produced in the collisional phase survive as mobile interstitials and vacancies as the cascade cools down to ambient temperature. Naturally, only the surviving defects can participate in defect-defect and defect-sink interactions and finally contribute to the accumulation of interstitials and vacancies in the medium.

A large fraction of the surviving defects form clusters due to their close proximity and high temperature during the thermal-spike phase of a cascade. Due to the localized and segregated production and different thermal stabilities of PICs and PVCs, defect clusters play a vital role in the defect accumulation process. While solving the conservation equations derived by Woo and Semenov [37] for the concentrations of two kinds of primary clusters, appropriate numerical methods for the system of ordinary differential equations (ODEs) are compared and the

validity of the methods is verified by applying them in the problem with a known solution. Thus, the evolution of microstructure such as PICs, PVCs and hence voids in 316 stainless steel as a function of irradiation dose is calculated.

Since the behaviour of defect accumulation is strongly dependent on the temperature, the calculation has been performed in three distinct temperature regions: low temperature, peak-swelling temperature and high temperature. It is found that the densities of primary clusters and defect contents in these clusters both initially increase with the irradiation dose, saturating at a relatively low dose ($<5x10^{-3}$ dpa). After that, the primary clusters keep a quasi-steady state between the creation by cascades and the annihilation with different processes. The removal of PVCs is attributed to massive vacancy evaporation from PVCs which contributes largely to the vacancy accumulation in the medium at elevated temperatures. Correspondingly, the removal of PICs can be realized by dislocation sweeping, the glide of PICs and absorption of evaporating vacancies in PICs. Due to the different annealing mechanisms of vacancies and interstitials in their primary clusters, the volume strain of voids has been accounted for. Therefore, the theory of production bias as a potent driving force for swelling and microstructural evolution can be used to describe the experimentally observed high swelling behaviour of voids at elevated temperatures which the traditional mean field theory is unable to unravel satisfactorily.

The calculated results are compared with the ones from previous Fokker-Planck analysis for the steady-state. Good agreement between the two approaches

is found.

Since the concept of production bias clearly describes the production, annihilation and accumulation of free defect fluxes, which are needed for characterizing microstructural developments in the medium under cascade conditions, it is suggested that the model be extended to investigate irradiation-induced creep, fracture, segregation, phase separation and precipitate coarsening.

Because the effect of gas pressure in voids which is important at high temperatures has not been included in the model due to the complication, the calculated void swelling is much underestimated in this temperature range. It was also mentioned before, that the process of void nucleation which is closely related to void swelling, has been neglected. Hence, it is recommended in further studies that:

a) the effects of gases in voids, in particular, helium gas be included in the current model to correctly reflect the behaviour of damage accumulation in reactor materials at high temperatures;

b) the problems of void nucleation and the dose dependence of the void density be dealt with even though they are not well understood and their effects cannot be easily quantified;

c) the strengths of various sinks as functions of temperature and dose be investigated because some sinks can be mostly dominant in one situation, others in another.

Furthermore, alloys normally possess complex composition and structure,

so that it is necessary that the effects of interogeneous material components such as grain boundaries, precipitates, solute segregation, impurities and surfaces be studied in order to have a more comprehensive model.

d) Further theoretical study of the convergence, stability and accuracy of the numerical methods for ODEs be conducted because of the steep change of primary cluster concentrations and void swelling in the present problem.

REFERENCES

[1] C. Cawthorne and E.J. Fulton, AERE-R5269, AERE Harwell (1966)446; Nature, **216**(1967)575.

[2] Proc. of the BNES European Conf. on Voids Formed by Irradiation of Reactor Materials at Reading University, 1971, S.F. Pugh, M.H. Lorretto and D.I.R. Norris, eds. Published by B.N.E.S.

[3] Proc. of Int. Conf. on Radiation Induced Voids in Metals at Albany, NY, 1972, J.W. Corbett and L.C. Ianniello, eds. Published by U.S.A.E.C.

[4] Proc. of Conf. on Defects and Defect Clusters in bcc Metals and their Alloys at N.B.S., Gaithersburg, MD, Nucl. Met. Vol.18, 1973.

[5] Proc. of Conf. on Physics of Voids at Harwell, UK, 1974, Ed. R.S. Nelson, (Harwell Res. Rep. AERE-R. 7934).

[6] Proc. of Int. Conf. on Fundamental Aspects of Radiation Damage in Metals at Gatlinburg, TN, 1975, M.T. Robinson and F.W. Young, eds. (U.S.E.R.D.A.).

[7] 13th Int. Sympoium on Radiation-Induced Changes in Microstructure at Seattle, WA, 1986, F.A. Garner, N.H. Packan and A.S. Kumar, eds. ASTM.

[8] Proc. of The Fifth Int. Conf. on Fusion Reactor Materials at Clearwater, FL,

1991, R.L. Klueh, R.E. Stoller and D.S. Gelles, eds.

[9] Proc. of Int. Conf. on Physics of Irradiation Effects in Metals, Szenes, G., Ed., Materials Science Forum. **97-99**(1992).

[10] Proc. of Int. Conf. on Evolution of Microstructure in Metals During Irradiation at Muskoka, Ont. Canada, 1992, Coleman, C.E., Holt, R.A. and Fleck, R.G., Eds., J. Nucl. Mater., **205**(1993).

[11] Proc. of Workshop on Time Dependence of Radiation Damage Accumulation and Its Impact on Materials Properties, Montreux, Switzerland, 1992, Gavillet, D., Victoria, M., Singh, B.N. and Horsewell, A., Eds., J. Nucl. Mater. **206**(1993).

[12] Norgett, M.J., Robinson, M.T. and Torrens, I.M., Nucl. Engng. Des., **33**(1976)50.

[13] Thompson, M.W., 1969, Defects and Radiation Damage in Metals, Cambridge University Press, P.144.

[14] Gibson, J.B., Goland, A.N., Milgram, M. and Vineyard, G.M., Phys. Rev. **120**(1960)1229.

[15] Scholz, A. and Lehmann, C., Phys. Rev. **B6**(1972)815.

[16] Robinson, M.T. and Torrens, I.M., Phys. Rev. Lett. **B9**(1974)5008.

[17] Heinisch, H.L., J. Nucl. Mater., **117**(1983)46.

[18] Heinisch, H.L. and Mann, F.M., J. Nucl. Mater., **122-123**(1984)1023.

[19] Diaz de la Rubia, T., Averback, R.S., Benedek, R. and Robertson, I.M., Radiat. Eff. Def. Sol., **113**(1990)39.

[20] Diaz de la Rubia and Guinan, M.W., Phys. Rev. Lett. **66**(1991)2766.

[21] English, C.A., Foreman, A.J.E., Phythian, W.J., Baco, D.J. and Jenkins, M.L., Mater. Sci. Forum, **97-99**(1992)1.

[22] Diaz de la Rubia, T. and Guinan, M.W., Mater. Sci. Forum, **97-99**(1992)23.

[23] Sigmund, P., Rev. Roum. Phys. **17**(1972)969.

[24] Merkle, K.L., Radiation Damage in Metals, American Society of Metals, Metals Park, Ohio, (1976)58.

[25] Ullmaier, H. and Schilling, W.," Radiation Damage in Metallic Reactor Materials", in Physics of Modern Materials, p.301 IAEA, Vienna, 1980.

[26] Woo, C.H. and Singh, B.N., Phys. stat. sol., **B159**(1990)609.

[27] Woo, C.H. and Singh, B.N., Phil. Mag., **A65**(1992)889.

[28] Bullough, R., Eyre, B.L. and Krishan, K., Proc. Roy. Soc., **A346**(1975)81.

[29] Heald, P.T. and Speight, M.V., J. Nucl. Mater., **64**(1977)139.

[30] Foreman, A.J.E. and Makin, M.J., J. Nucl. Mater., **79**(1979)43.

[31] Grasse, D., von Guerard, B. and Peisl, J., J. Nucl. Mater. **120**(1984)304.

[32] Rauch, R., Peisl, J., Schmalzbauer, A. and Wallner, G., J. Nucl. Mater. **168**(1989)101.

[33] Woo, C.H., Singh, B.N. and Heinisch, H.L., J. Nucl. Mater., **174**(1990)190.

[34] English, C.A., Phythian, W.J. and Foreman, A.J.E., J. Nucl. Mater., **174**(1990)135.

[35] Trinkaus, H., Singh, B.N. and Woo, C. H., J. Nucl. Mater., **212-215**(1994)18.

[36] Singh, B.N., Woo, C.H. and Foreman, A.J.E., Mater. Sci. Forum. **97-**

99(1992)75.

[37] Woo, C.H. and Semenov, A.A., Phil. Mag., **A67**(1993)1247.

[38] Woo, C,H., Singh, B,N. and Garner, F,A., J. Nucl. Mater. **191-194**(1992)1224.

[39] Holt, R.A., Woo, C.H. and Chow, C.K., J. Nucl. Mater., **205**(1993)293.

[40] Woo, C.H., Phil. Mag., **A70**(1994)713.

[41] Semenov, A. A. and Woo, C.H., J. Nucl. Mater., **212-215**(1994)310

[42] Singh, B.N., Trinkaus, H. and Woo, C.H., J. Nucl. Mater., **212-215**(1994)168.

[43] Woo, C.H., Semenov, A.A. and Singh, B.N., J. Nucl. Mater. **206**(1993)170.

[44] Semenov, A.A. and Woo, C.H., J. Nucl. Mater., **205**(1993)74.

[45] Johnson, R.A. and Orlow, A.N., 1986., Physics of Radiation Effects in Crystals, North-Holland Physics Publishing, p.189.

[46] Kapinos, V.G. and Bacon, D.J., Phil. Mag. **A68**(1993)1165.

[47] Barbu A. and Martin G., Solid State Phenomena, **30** & **31**(1993)179.

[48] Mansure, L.K., "Mechanism and Kinetics of Radiation Effects" in Metals and Alloys in Kinetics of Nonhomogenous Processes, Edited by Freeman, G.R., John Wiley & Sons Inc., New York, 1987, P377-463.

[49] Brailsford, A.D. and Bullough, R., J. Nucl. Mater. **69-70**(1978)434., J. Nucl. Mater. **42**(1972)121.

[50] Atkinson L. V., Harley P.J. and Hudson J. D., 1989., Numerical Methods with Fortran 77, Addison-Wesley Publishing Company, p.299.

[51] Press, W.H., Flannery, B.P., Teukolsky, S.A. and Vetterling, W.T., 1989, Numerical Recipes (FORTRAN version), Cambridge University Press, p.572.

[52] IMSL MATH/LIBRARY User's Manual, Vol.2, Version 1.1, 1989, IMSL Inc. p.629.

[53] John, R. R., 1983., Numerical Methods, Software, and Analysis, McGraw-Hill Book Company, p.265.

[54] Gene, H. G. and James, M. O., 1992., Scientific Computing and Differential Equations, Academic Press Inc., p.15.

[55] Fox, L. and Mayers. D.F., 1987., Numerical Solution of Ordinary Differential Equations, Chapman and Hall Ltd, p.206.

[56] "Energy in Transition: 1985-2010", Committee on Nuclear and Alternative Energy Systems, National Research Council, National Academy of Sciences, Washington, DC, 1979.

[57] Skinner, B.C. and Woo, C.H., Phys. Rev. **B30**(1984)3084.

[58] Stoller, R.E. and Odette, G.E., 1987, ASTM STP 955, edited by F.A. Garner, N.H. Packan and A.S. Kumar (Philadelphia, Pennsylvania; ASTM), P. 371

[59] Parker, C.A. and Russell, K.C., Scripta Metallurgica, **15**(1981)643.

[60] Brailsford, A.D. and Bullough, R., The Theory of Sink Strengths, AERE Harwell Report TP.854, 1980.

[61] Assassa, W. and Guiraldenq, P., Metal Science, **12**(1978)123.

[62] Rothman, S.J., Nowicki, L.J. and Murch, G.E., J. Physics F: Metal Physics, **10**(1980)383.

[63] Murr, L.E., Wong, G.I. and Horylev, R.J., Acta Metallurgia, **21**(1973)593.

[64] Schramm, R.E. and Reed, R.P., Met. Trans., **6A**(1975)1343.

[65] Mansur, L.K. and Coghlan, W.A., J. Nucl. Mater., **119**(1983)1.

[66] Stoller, R.E. and Odette, G.R., J. Nucl. Mater., **131**(1985)118.

[67] Stoller, R.E. and Odette, G.R., J. Nucl. Mater., **103-104**(1981)1361.

[68] Stoller, R.E., PhD. Thesis, Univ. Calif. Santa Barbara, 1987.

[69] Peterson, N.L., J. Nucl. Mater., **69&70**(1978)3.

[70] LeClaire, A.D., J. Nucl. Mater., **69&70**(1978)70.

[71] Perkins, R.A., Met. Trans., **4**(1973)1665.

[72] Perkins, R.A., Padgett, R.A. and Tunali, N.K., Met. Trans., **4**(1973)2535.

[73] Garner, F.A., and Wolfer, W.G., J. Nucl. Mater., **122&123**(1984)201.

[74] Murr, L.E., Interfacial Phenomena in Metals and Alloys, Addison-Wesley, Reading, 1975.

[75] Zinkle, S.J., and Singh, B.N., J. Nucl. Mater., **199**(1993)173.

[76] Lam, N.Q., Doan, N.V. and Dagens, L., J. Phys., **F5**(1985)799.

[77] Lam, N.Q., and Dagens, L., J. Phys., **F16**(1986)1373.

[78] Simons, R.L., J. Nucl. Mater., **141-143**(1986)665.

[79] Trankaus, H., Singh, B.N. and Foreman, A.J.E., J. Nucl. Mater., **199**(1992)1., **206**(1993)200.

[80] Kroupa, F., Phil. Mag., **7**(1962)783.

[81] Friedel, J., Dislocations, 1964, Pergomon Press (Addison Wesley), P.380.

[82] Friedel, J., Electron Microscopy and Strength of Crystals., eds. Thomas, G.

and Wasburn, J., New York, Interscience, 1963, p.605.

[83] Mott, N.F., Imperfections in Neraly Perfect Crystals, eds. Shockley, W. et. al., New York, John Willey, 1952, p.173.

[84] Odette, G.R., Maziasz, P.J. and Spitznagel, J.A., J. Nucl. Mater. **103&104**(1981)1289.

[85] Singh, B.N. and Foreman, A.J.E., J. Nucl. Mater., **103&104**(1981)1469.

APPENDIX A

PROGRAM FOR SOLVING THE SYSTEM OF DIFFERENTIAL EQUATIONS

This appendix lists the program which was used to calculate the number densities of primary interstitial clusters N_{ic} and primary vacancy clusters N_{vc}; the total interstitial contents Q_i and the total vacancy contents in their respective clusters; void swelling S; void swelling rate dS/Kdt as a function of irradiation dose (in NRT dpa) at different temperatures. The program solves the system of ordinary differential equations (2.9)-(2.13), given in chapter two.

Given values for 5 variables y known at x, use the Runge-Kutta method or method for stiff equations to advance the solution over an interval h and return the incremented variables as new y. The subroutine funct(y,r,f,dr) returns derivatives f and dr at new x.

Program Listing

```
      PROGRAM TIMDEP
C     Runge-Kutta method
      DIMENSION Y(5),YT(5),DYT(5),DYM(5),DYDT(5)
      COMMON/P/P,Z,TK,TC ,PI
      COMMON/G/G,EPSI,EPSV,ANC
      COMMON/E/DV0,ESD,DE
      COMMON/CD/B0,RI0,RV0,W,OMEGA,SNI0,SNV0
      OPEN (UNIT=44,FILE='dat.506')
C                                        material and irradiation parameters
      PI=3.14159E0
      B0=2.53E-10
      P=0.3E0
      Z=2.E0
      G=1.E-7
      EPSI=0.45E0
      EPSV=0.5E0
      RI0=2.E0*B0
      RV0=3.E0*B0
      ESD=4.80653E-19
      DE=4.80653E-20
      TC=500.E0
      TK=TC+273.E0
      W=10.E0*B0*B0
      OMEGA=11.5E-30
      ANC=2.53E+26*EXP(-2.3E-2*TC)
      SNI0=PI*RI0*RI0*B0/OMEGA
      SNV0=PI*RV0*RV0*B0/OMEGA
C                                        initial conditions
      GDPA=0.E0
      Y(1)=0.E0
      Y(2)=0.E0
      Y(3)=0.E0
      Y(4)=0.E0
      R=15.E-10
C                                        integration loop
      DO 5 I=1,300000
      H=1.E-5
      HH=H*0.5E0
      H6=H/6.E0
```

```
C                                          initialize Runge-Kutta method
      CALL FUNCTI(Y,DYDT)
      DO 10 J=1,5
      YT(J)=Y(J)+HH*DYDT(J)
10    CONTINUE
      CALL FUNCT(YT,DYT)
      DO 20 K=1,5
      YT(K)=Y(K)+HH*DYT(K)
20    CONTINUE
      CALL FUNCT(YT,DYM)
      DO 22 M=1,5
      YT(M)=Y(M)+H*DYM(M)
      DYM(M)=DYT(M)+DYM(M)
22    CONTINUE
      CALL FUNCT(YT,DYT)
      DO 24 N=1,5
      Y(N)=Y(N)+H6*(DYDT(N)+DYT(N)+2*DYM(N))
24    CONTINUE
      GDPA=GDPA+H
      DPA=GDPA*10.E0
      S=4.E0*PI*ANC/3.E0*R*R*R
      DSDGT=4.E0*PI*ANC*R*R*DR
      DSDKT=DSDGT/10.E0
      DO 30 J=1,4
      Y(J)=Y(J)/OMEGA
30    CONTINUE
      Y(5)=Y(2)-Y(4)
      Y(6)=Y(1)-Y(3)
C                                          write output
      WRITE(44,'(E10.3,2E12.4)')DPA,S,DSDKT
C     WRITE(44,'(E10.3,6E12.4)')DPA,(Y(K),K=1,6)
      DO 40 K=1,4
      Y(K)=Y(K)*OMEGA
40    CONTINUE
5     CONTINUE
      STOP
      END
C
      SUBROUTINE FUNCT(Y,DYDT)
      DIMENSION Y(5),DYDT(5)
      COMMON/P/P,Z,TK,TC,PI
      COMMON/G/G,EPSI,EPSV,ANC
      COMMON/E/DV0,ESD,DE
```

```
      COMMON/CD/B0,RI0,RV0,W,OMEGA,SNI0,SNV0
C                                          material parameters
      AK=1.380658E-23
      BETA=1.E0/AK/TK
      GAMA=1.4E-3*TC
      DV0=8.E-5
      DCVE=DV0*EXP(-ESD*BETA)
      EDE=EXP(DE*BETA)
      EC=EXP(2.E0*GAMA*OMEGA*BETA/Y(5))
C                                          sink strengths
      AKN=6.8E+16*Z*EXP(-9.6E-3*TC)
      AKC=4.E0*PI*ANC*Y(5)
      AKIL=5.E+27*Z*EXP(-0.0327*TC)*SQRT(Z*PI/AKN)
      AKIC=2.E0*Z*SQRT(PI*Y(1)*Y(2)/B0/OMEGA)
      AKVC=2.E0*Z*SQRT(PI*Y(3)*Y(4)/B0/OMEGA)
      AKCD=AKIC+AKVC
      AKD=AKN+AKIL+AKCD
      AKV=AKC+AKD
      AKI=AKV+P*AKD
      PA=P*AKC/AKI
C                                          vacancy emission strengths
      GEC=AKC*DCVE*EC
      GEN=AKN*DCVE
      GEIL=AKIL*DCVE
      GEVC=AKVC*DCVE*EDE
      GEIC=AKIC*DCVE/EDE
      GE=GEC+GEN+GEIL+GEVC+GEIC
      EPSVP=EPSV-GE/G
C                                          fluxes of point defects
      FJVCE=Z*DCVE*EDE/G
      FJICE=Z*DCVE/EDE/G
      FJI0=Z*(1.E0+PA)*(1.E0-EPSI)/AKV
      FJV0=Z*(1.E0-EPSVP)/AKV
C                                          lifetimes of defect clusters
      RTJD=(AKN+AKIL)/Z*W
      RTIS=(FJV0-FJI0-FJICE)/B0/RI0
      RTVS=(FJI0-FJV0+FJVCE)/B0/RV0
C                                  evaluations of right-hand side functions
      IF (RTIS.GT.1.E-8) THEN
      DYDT(1)=EPSI/SNI0-(RTIS+RTJD/G)*Y(1)
      ELSE
      DYDT(1)=EPSI/SNI0-RTJD/G*Y(1)
      END IF
```

```
      IF (RTVS.GT.1.E-8) THEN
      DYDT(3)=EPSV/SNV0-(RTVS+RTJD/G)*Y(3)
      ELSE
      DYDT(3)=EPSV/SNV0-(RTJD/G*Y(3)
      END IF
      IF (Y(2).GT.1.E-8) THEN
      DYDT(2)=EPSI
     * -Y(2)*2.E0*RI0*RTIS*SQRT(PI*B0/OMEGA*Y(1)/Y(2))-Y(2)*RTJD/G
      ELSE
      DYDT(2)=EPSI-RTJD/G*Y(2)
      END IF
      IF (Y(4).GT.1.E-8) THEN
      DYDT(4)=EPSV
     * -Y(4)*2.E0*RV0*RTVS*SQRT(PI*B0/OMEGA*Y(3)/Y(4))-Y(4)*RTJD/G
      ELSE
      DYDT(4)=EPSV-RTJD/G*Y(4)
      END IF
      DYDT(5)=((EPSI-EPSVP)/AKV+P*(1.E0-EPSI)*AKD/AKV/AKI
     *  -DCVE*EC/G)/Y(5)
      RETURN
      END
```

APPENDIX B

Input Parameters

The descriptions and symbols of input parameters in the context are listed in the right column in Table B, along with their symbols and values in the fortran program listed in the left column. These values are for 316 stainless steel.

Table B Description of Input Parameters

Symbol	Value	Description
B0	2.53×10^{-10} m	Jump distance for vacancies and interstitials, $b^{(a)}$.
OMEGA	1.15×10^{-29} m^3	Atomic volume, $\Omega^{(c)}$.
P	0.3	Dislocation bias, $p^{(b)}$.
Z	2	Dislocation bias factor for vacancies, $Z^{(b)}$.
K	10^{-6}dpa.s^{-1}	Point defect production rate, $K^{(a)}$.
G	10^{-7}dpa.s^{-1}	Effective point defect generation rate, $G^{(a)}$.
EPSI	5	Intracascade interstitial clustering fraction, $\varepsilon_i^{(a)}$.
EPSV	0.5	Intracascade vacancy clustering fraction, $\varepsilon_v^{(a)}$.
RI0	2b	Initial radius of PICs, $r_{i0}^{(a)}$.
RV0	3b	Initial radius of PVCs, $r_{v0}^{(a)}$.
W	$10\text{-}20b^2$	Reaction constant for dislocation lines and PICs or PVCs, $W=W_i=W_v^{(a)}$.
ESD	3eV	Activation energy for self-diffusion, $(E_v^m+E_v^f)^{(c)}$.
DE	0.3eV	Average loop-line energy, $\Delta E^{(d)}$.
OMEGA	11.5×10^{-30} m^3	Atomic volume, $\Omega^{(c)}$.
R_0	$5\text{-}30\times10^{-10}$ m	Average initial radius of voids, $r_{c0}^{(a)}$.
DV0	8×10^{-5} $m^2.s^{-1}$	Vacancy diffusivity pre-exponential, $D_{v0}^{(a)}$.
BETA	$(KT)^{-1}$	K is Boltzman's constant and T is absolute temperature, β.

(a) Data from Woo and Semenov (1993)
(b) Data from Skinner and Woo (1984)
(c) Data from Stoller and Odette (1987)
(d) Data from Foreman and Makin (1979)

APPENDIX C

Output Parameters

The descriptions and symbols of output parameters in the context are listed in the right column, along with their symbols and values in the fortran program listed in the left column. These values are for 316 stainless steel.

Table C Description of Output Parameters

Symbol	Unit	Description
DOSE	10^{-3}-50 dpa	Irradiation dose.
S	%	Change of void volume, or void swelling, S.
DSDKT	dpa^{-1}	Change rate of void volume, or void swelling rate, dS/Kdt.
Y(1)	m^{-3}	Number density of PICs, N_{ic}.
Y(2)	m^{-3}	Total interstitial content in the PICs, Q_i.
Y(3)	m^{-3}	Number density of PVCs, N_{vc}.
Y(4)	m^{-3}	Total vacancy content in the PVCs, Q_v.

APPENDIX D

A Typical Sample of Output Data

This is a sample of output data directly computed from the program listed in Appendix A. It records the corresponding changes of N_{ic}, Q_i, N_{vc}, Q_v, S and DSDKT (right six columns) when irradiation dose (first column) increases steadily. In this sample, T_c is the temperature and R_0 is the average initial radius of voids. The first column represents the steady change of the amount of irradiation dose in unit NRT dpa.

Table D

T_c	R_0
0.50E+03	0.15E+02

DOSE	N_{ic}	Q_i	N_{vc}	Q_v	S	DSDKT
0.100E-03	0.212E+23	0.374E+24	0.959E+22	0.352E+24	0.363E-04	0.433E-03
0.200E-03	0.403E+23	0.701E+24	0.169E+23	0.563E+24	0.364E-04	0.782E-03
0.300E-03	0.574E+23	0.980E+24	0.226E+23	0.687E+24	0.365E-04	0.963E-03
0.400E-03	0.725E+23	0.122E+25	0.271E+23	0.754E+24	0.366E-04	0.105E-02
0.500E-03	0.859E+23	0.141E+25	0.305E+23	0.784E+24	0.367E-04	0.109E-02
0.600E-03	0.979E+23	0.158E+25	0.331E+23	0.791E+24	0.368E-04	0.110E-02
0.700E-03	0.109E+24	0.173E+25	0.352E+23	0.785E+24	0.369E-04	0.110E-02
0.800E-03	0.118E+24	0.185E+25	0.368E+23	0.772E+24	0.370E-04	0.108E-02

0.900E-03 0.127E+24 0.196E+25 0.380E+23 0.755E+24 0.371E-04 0.106E-02
0.100E-02 0.135E+24 0.206E+25 0.389E+23 0.738E+24 0.372E-04 0.104E-02
0.110E-02 0.142E+24 0.214E+25 0.395E+23 0.721E+24 0.373E-04 0.101E-02
0.120E-02 0.148E+24 0.221E+25 0.401E+23 0.706E+24 0.374E-04 0.991E-03
0.130E-02 0.154E+24 0.228E+25 0.404E+23 0.694E+24 0.375E-04 0.971E-03
0.140E-02 0.160E+24 0.234E+25 0.407E+23 0.683E+24 0.376E-04 0.953E-03
0.150E-02 0.164E+24 0.239E+25 0.409E+23 0.673E+24 0.377E-04 0.937E-03
0.160E-02 0.169E+24 0.244E+25 0.411E+23 0.666E+24 0.378E-04 0.922E-03
0.170E-02 0.173E+24 0.248E+25 0.412E+23 0.660E+24 0.379E-04 0.910E-03
0.180E-02 0.177E+24 0.251E+25 0.412E+23 0.655E+24 0.380E-04 0.899E-03
0.190E-02 0.180E+24 0.255E+25 0.413E+23 0.651E+24 0.380E-04 0.889E-03
0.200E-02 0.183E+24 0.258E+25 0.413E+23 0.648E+24 0.381E-04 0.881E-03
0.210E-02 0.186E+24 0.260E+25 0.413E+23 0.645E+24 0.382E-04 0.874E-03
0.220E-02 0.189E+24 0.263E+25 0.413E+23 0.643E+24 0.383E-04 0.867E-03
0.230E-02 0.191E+24 0.265E+25 0.414E+23 0.642E+24 0.384E-04 0.862E-03
0.240E-02 0.193E+24 0.267E+25 0.413E+23 0.641E+24 0.385E-04 0.857E-03
0.250E-02 0.195E+24 0.269E+25 0.413E+23 0.640E+24 0.386E-04 0.853E-03
0.260E-02 0.197E+24 0.270E+25 0.413E+23 0.639E+24 0.387E-04 0.849E-03
0.270E-02 0.198E+24 0.271E+25 0.413E+23 0.638E+24 0.387E-04 0.846E-03
0.280E-02 0.200E+24 0.273E+25 0.413E+23 0.638E+24 0.388E-04 0.844E-03
0.290E-02 0.201E+24 0.274E+25 0.413E+23 0.637E+24 0.389E-04 0.841E-03
0.300E-02 0.202E+24 0.275E+25 0.413E+23 0.637E+24 0.390E-04 0.839E-03
0.310E-02 0.204E+24 0.275E+25 0.413E+23 0.637E+24 0.391E-04 0.838E-03
0.320E-02 0.205E+24 0.276E+25 0.413E+23 0.636E+24 0.392E-04 0.836E-03
0.330E-02 0.206E+24 0.277E+25 0.413E+23 0.636E+24 0.392E-04 0.835E-03
0.340E-02 0.206E+24 0.277E+25 0.413E+23 0.636E+24 0.393E-04 0.834E-03
0.350E-02 0.207E+24 0.278E+25 0.413E+23 0.636E+24 0.394E-04 0.833E-03
0.360E-02 0.208E+24 0.278E+25 0.413E+23 0.636E+24 0.395E-04 0.832E-03
0.370E-02 0.209E+24 0.279E+25 0.413E+23 0.636E+24 0.396E-04 0.832E-03
0.380E-02 0.209E+24 0.279E+25 0.413E+23 0.636E+24 0.397E-04 0.832E-03
0.390E-02 0.210E+24 0.279E+25 0.413E+23 0.636E+24 0.397E-04 0.831E-03
0.400E-02 0.210E+24 0.280E+25 0.413E+23 0.636E+24 0.398E-04 0.831E-03
0.410E-02 0.211E+24 0.280E+25 0.413E+23 0.635E+24 0.399E-04 0.831E-03
0.420E-02 0.211E+24 0.280E+25 0.412E+23 0.635E+24 0.400E-04 0.831E-03
0.430E-02 0.211E+24 0.280E+25 0.412E+23 0.635E+24 0.401E-04 0.831E-03
0.440E-02 0.212E+24 0.280E+25 0.412E+23 0.635E+24 0.402E-04 0.831E-03
0.450E-02 0.212E+24 0.281E+25 0.412E+23 0.635E+24 0.402E-04 0.831E-03
0.460E-02 0.212E+24 0.281E+25 0.412E+23 0.635E+24 0.403E-04 0.832E-03
0.470E-02 0.213E+24 0.281E+25 0.412E+23 0.635E+24 0.404E-04 0.832E-03
0.480E-02 0.213E+24 0.281E+25 0.412E+23 0.635E+24 0.405E-04 0.832E-03
0.490E-02 0.213E+24 0.281E+25 0.412E+23 0.635E+24 0.406E-04 0.833E-03
0.500E-02 0.213E+24 0.281E+25 0.412E+23 0.635E+24 0.407E-04 0.833E-03
0.510E-02 0.213E+24 0.281E+25 0.412E+23 0.635E+24 0.407E-04 0.834E-03

0.520E-02 0.214E+24 0.281E+25 0.412E+23 0.635E+24 0.408E-04 0.834E-03
0.530E-02 0.214E+24 0.281E+25 0.412E+23 0.635E+24 0.409E-04 0.835E-03
0.540E-02 0.214E+24 0.281E+25 0.412E+23 0.635E+24 0.410E-04 0.835E-03
0.550E-02 0.214E+24 0.281E+25 0.412E+23 0.635E+24 0.411E-04 0.836E-03
0.560E-02 0.214E+24 0.281E+25 0.412E+23 0.635E+24 0.412E-04 0.836E-03
0.570E-02 0.214E+24 0.281E+25 0.412E+23 0.635E+24 0.412E-04 0.837E-03
0.580E-02 0.214E+24 0.281E+25 0.412E+23 0.635E+24 0.413E-04 0.837E-03
0.590E-02 0.214E+24 0.281E+25 0.412E+23 0.635E+24 0.414E-04 0.838E-03
0.600E-02 0.214E+24 0.281E+25 0.412E+23 0.635E+24 0.415E-04 0.839E-03
0.610E-02 0.214E+24 0.281E+25 0.412E+23 0.635E+24 0.416E-04 0.839E-03
0.620E-02 0.214E+24 0.281E+25 0.412E+23 0.635E+24 0.417E-04 0.840E-03
0.630E-02 0.215E+24 0.281E+25 0.412E+23 0.635E+24 0.417E-04 0.841E-03
0.640E-02 0.215E+24 0.281E+25 0.412E+23 0.635E+24 0.418E-04 0.841E-03
0.650E-02 0.215E+24 0.281E+25 0.412E+23 0.635E+24 0.419E-04 0.842E-03
0.660E-02 0.215E+24 0.281E+25 0.412E+23 0.635E+24 0.420E-04 0.843E-03
0.670E-02 0.215E+24 0.281E+25 0.412E+23 0.635E+24 0.421E-04 0.843E-03
0.680E-02 0.215E+24 0.281E+25 0.412E+23 0.635E+24 0.422E-04 0.844E-03
0.690E-02 0.215E+24 0.281E+25 0.412E+23 0.635E+24 0.422E-04 0.845E-03
0.700E-02 0.215E+24 0.281E+25 0.412E+23 0.635E+24 0.423E-04 0.845E-03
0.710E-02 0.215E+24 0.281E+25 0.412E+23 0.635E+24 0.424E-04 0.846E-03
0.720E-02 0.215E+24 0.281E+25 0.412E+23 0.635E+24 0.425E-04 0.847E-03
0.730E-02 0.215E+24 0.281E+25 0.412E+23 0.635E+24 0.426E-04 0.847E-03
0.740E-02 0.215E+24 0.281E+25 0.412E+23 0.635E+24 0.427E-04 0.848E-03
0.750E-02 0.215E+24 0.281E+25 0.412E+23 0.635E+24 0.428E-04 0.849E-03
0.760E-02 0.215E+24 0.281E+25 0.412E+23 0.635E+24 0.428E-04 0.850E-03
0.770E-02 0.215E+24 0.281E+25 0.412E+23 0.635E+24 0.429E-04 0.850E-03
0.780E-02 0.215E+24 0.281E+25 0.412E+23 0.635E+24 0.430E-04 0.851E-03
0.790E-02 0.215E+24 0.281E+25 0.412E+23 0.635E+24 0.431E-04 0.852E-03
0.800E-02 0.215E+24 0.281E+25 0.412E+23 0.635E+24 0.432E-04 0.852E-03
0.810E-02 0.215E+24 0.281E+25 0.412E+23 0.635E+24 0.433E-04 0.853E-03
0.820E-02 0.215E+24 0.281E+25 0.412E+23 0.635E+24 0.433E-04 0.854E-03
0.830E-02 0.215E+24 0.281E+25 0.412E+23 0.635E+24 0.434E-04 0.855E-03
0.840E-02 0.215E+24 0.281E+25 0.412E+23 0.635E+24 0.435E-04 0.855E-03
0.850E-02 0.215E+24 0.281E+25 0.412E+23 0.635E+24 0.436E-04 0.856E-03
0.860E-02 0.215E+24 0.281E+25 0.412E+23 0.635E+24 0.437E-04 0.857E-03
0.870E-02 0.215E+24 0.281E+25 0.412E+23 0.635E+24 0.438E-04 0.857E-03
0.880E-02 0.215E+24 0.281E+25 0.412E+23 0.635E+24 0.439E-04 0.858E-03
0.890E-02 0.215E+24 0.281E+25 0.412E+23 0.635E+24 0.439E-04 0.859E-03
0.900E-02 0.215E+24 0.281E+25 0.412E+23 0.635E+24 0.440E-04 0.859E-03
0.910E-02 0.215E+24 0.281E+25 0.412E+23 0.635E+24 0.441E-04 0.860E-03
0.920E-02 0.215E+24 0.281E+25 0.412E+23 0.635E+24 0.442E-04 0.861E-03
0.930E-02 0.215E+24 0.281E+25 0.412E+23 0.635E+24 0.443E-04 0.862E-03
0.940E-02 0.215E+24 0.281E+25 0.412E+23 0.635E+24 0.444E-04 0.862E-03

0.950E-02 0.215E+24 0.281E+25 0.412E+23 0.635E+24 0.445E-04 0.863E-03
0.960E-02 0.215E+24 0.281E+25 0.412E+23 0.635E+24 0.446E-04 0.864E-03
0.970E-02 0.215E+24 0.281E+25 0.412E+23 0.635E+24 0.446E-04 0.864E-03
0.980E-02 0.215E+24 0.281E+25 0.412E+23 0.635E+24 0.447E-04 0.865E-03
0.990E-02 0.215E+24 0.281E+25 0.412E+23 0.635E+24 0.448E-04 0.866E-03
0.100E-01 0.215E+24 0.281E+25 0.412E+23 0.635E+24 0.449E-04 0.867E-03